G protein subunit *Gγ13*-mediated signaling pathway is critical to the inflammation resolution and functional recovery of severely injured lungs

Yi-Hong Li[1], Yi-Sen Yang[1], Yan-Bo Xue[1], Hao Lei[1], Sai-Sai Zhang[1], Junbin Qian[2,3,4], Yushi Yao[5], Ruhong Zhou[1,6*§], Liquan Huang[1,6,7*§¶]

***For correspondence:** huangliquan@zju.edu.cn (LH); rhzhou@zju.edu.cn (RZ)

Present address: [§]College of Life Sciences, Zhejiang University, China; [¶]Chemical Senses Center, Chemical Senses Center, United States

[1]College of Life Sciences, Zhejiang University, Hangzhou, Zhejiang 310058, P. R. China; [2]Zhejiang Provincial Key Laboratory of Precision Diagnosis and Therapy for Major Gynecological Diseases, Women's Hospital, Zhejiang University School of Medicine, Hangzhou, Zhejiang 310058, P.R. China; [3]Institute of Genetics, Zhejiang University School of Medicine, Hangzhou, Zhejiang 310058, P.R. China; [4]Cancer Center, Zhejiang University, Hangzhou, Zhejiang 310058, P.R. China; [5]Institute of Immunology and Sir Run Run Shaw Hospital, Zhejiang University school of Medicine, Hangzhou, Zhejiang 310058, P.R. China; [6]Zhejiang University Shanghai Institute for Advanced Study, Shanghai, Shanghai 201203, P.R. China; [7]Monell Chemical Senses Center, c, PA 19104, United States

Abstract Tuft cells are a group of rare epithelial cells that can detect pathogenic microbes and parasites. Many of these cells express signaling proteins initially found in taste buds. It is, however, not well understood how these taste signaling proteins contribute to the response to the invading pathogens or to the recovery of injured tissues. In this study, we conditionally nullified the signaling G protein subunit *Gγ13* and found that the number of ectopic tuft cells in the injured lung was reduced following the infection of the influenza virus H1N1. Furthermore, the infected mutant mice exhibited significantly larger areas of lung injury, increased macrophage infiltration, severer pulmonary epithelial leakage, augmented pyroptosis and cell death, greater bodyweight loss, slower recovery, worsened fibrosis and increased fatality. Our data demonstrate that the *Gγ13*-mediated signal transduction pathway is critical to tuft cells-mediated inflammation resolution and functional repair of the damaged lungs.To our best knowledge, it is the first report indicating subtype-specific contributions of tuft cells to the resolution and recovery.

Introduction

The respiratory system comprises the nasal cavity, airways, and lungs, and has the largest surface area exposed to the external environment. It is thus constantly challenged by various stimuli, ranging from odorants, pollutants, toxins, allergens, to viruses, bacteria, and fungi. Prompt detection and appropriate responses to harmful inhalants are critical to maintaining not only the pivotal gas-

exchange function of the system but also the overall health or even vitality of an individual. How the host responds to the external challenges and what damages can be inflicted upon the host depend on the types of harmful stimulus, dosage, host genetic background and immune history (***Yunis et al. 2023***).

Over the past decades, viral infection has been salient risks to human health. The severe acute respiratory syndrome coronavirus (SARS-CoV-1), and H1N1 influenza A virus and SARS-CoV2 have caused pandemics (***Peiris 2003***; ***Donaldson et al. 2009***; ***Chen et al. 2020***). However, it remains elusive how the host and infectious viruses interact and how the host regulates its responses to the invasion. Both under- and over-reactions by the host appear to engender serious consequences.

Recent studies have shown that several types of epithelial cells expressing the chemosensory receptors play important roles in detecting and responding to the external stimuli in the respiratory system (***Carey and Lee 2019***;***Tizzano and Finger 2013***). Among them is a rare type of microvillous cells, tuft cells (***Billipp et al. 2021***), which have also been found in a number of tissues, including the gastrointestinal tract, pancreas, respiratory airways and lungs, gallbladder and thymus (***Bezencon et al. 2008***; ***Miller et al. 2018***; ***Montoro et al. 2018***; ***Nevalainen 1977***; ***Saqui-Salces et al. 2011***; ***DelGiorno et al. 2020***). These cells can sense noxious stimuli and invading pathogens, such as allergens, bacteria, protists and helminths (***Gerbe et al. 2016***; ***Howitt et al. 2016***; ***Lei et al. 2018***; ***Luo et al. 2019***; ***von Moltke et al. 2016***). Tuft cells are known to express canonical chemosensory signaling pathways, including the sweet and umami taste receptor subunit Tas1r3 (***Howitt et al. 2020***), bitter taste receptors Tas2rs (***Luo et al. 2019***; ***Imai et al. 2020***), and olfactory receptors Vmn2r26 (***Xiong et al. 2022***), as well as their downstream signaling proteins including the heterotrimeric G protein subunits α-gustducin, Gβ1 and Gγ13, phospholipases, and the transient receptor potentialion channel *Trpm5* (***Howitt et al. 2016***; ***Doyle et al. 2023***). Even the signal transduction of the Sucnr1 receptor for succinic acid and free fatty acid receptor 2 Ffar2 for propionate, characteristic metabolites of certain microbes, is mediated by α-gustducin and / or *Trpm5* signaling proteins to monitor changes in gut microbiota and airway infection. And ablation of either α-gustducin or *Trpm5* diminishes the intestinal and tracheal epithelia's responses to the infection of the parasitic helminths and microbial colonization (***Lei et al. 2018***; ***Nadjsombati et al. 2018***; ***Schneider et al. 2018***; ***Keshavarz et al. 2022***; ***Perniss et al. 2023***).

Once stimulated, tuft cells can release a number of output signaling molecules, including IL-25, prostaglandins (***Kotas et al. 2022***), cysteinyl leukotrienes (***Bankova et al. 2018***; ***Bankova and Boyce 2018***; ***McGinty et al. 2020***), acetylcholine (***Hollenhorst et al. 2020***;***Krasteva et al. 2011***), and other substances, to stimulate type 2 innate lymphoid cells, nerve terminals or adjacent cells, initiating innate and adaptive immune responses, leading to the elimination of irritants and pathogens, and eventually to tissue repair and remodeling (***Finger et al. 2003***; ***Tizzano et al. 2010***; ***Saunders et al. 2014***). However, tuft cells are heterogeneous in terms of gene expression patterns, signal transduction pathways and output effectors (***Banerjee et al. 2018***). For example, some tuft cells express subsets of Tas2r receptors, or cysteinyl leukotriene receptor 3 (Cysltr3) while others do not (***Luo et al. 2019***; ***Imai et al. 2020***; ***Bankova et al. 2018***). It seems important to determine ligand profiles, output signals and physiological roles for tuft cells residing in different tissues to fully understand their protective functions against various pathogens and at different stages of disease progression.

Although they are normally only found in the nasal cavity and trachea, rarely found distal to the lung hilus (***Krasteva et al. 2011***; ***Tizzano et al. 2010***; ***Saunders et al. 2014***), tuft cells can be ectopically formed in the distal lung following severe viral infection or chemical damage (***Rane et al. 2019***; ***Barr et al. 2022***; ***Roach et al. 2022***; ***Melms et al. 2021***). These ectopic tuft cells of molecular diversities emerge around 12 days post viral infection, suggesting that they may not play any role in the initial response to the infection or during viral clearance (***Rane et al. 2019***; ***Barr et al. 2022***). However, it is unclear whether each subtype of these diverse tuft cells makes unique contributions to the subsequent inflammation resolution, tissue repair and remodeling. In this study, we conditionally nullified the expression of a heterotrimeric G protein subunit, *Gγ13*, in the choline acetyltransferase (ChAT)-expressing tuft cells, which resulted in the generation of

fewer tuft cells, but conferred even severer injury, slower recovery and higher fatality following the H1N1 influenza infection. Our data indicate that subsets of ectopic tuft cells with or without *Gγ13* expression play different important roles in the inflammation resolution and tissue repair.

Results

Severe injury induces the generation of taste signaling proteins-expressing ectopic tuft cells

To verify the previously reported ectopic generation of lung tuft cells upon severe injury, we intranasally inoculated adult mice with a sublethal dose of H1N1 viruses, and observed the bodyweight changes over a course of 25 days post infection (dpi) (***Figure 1***A). The mice were then killed and their lungs were dissected out for analyses (***Figure 1***A). The mice showed bodyweight loss over the days post infection with a peak loss of up to 25% of their original bodyweight around 8 to 9 dpi, and their lungs displayed lesion areas, of which the histological analysis showed massive alveolar damage and severe epithelial dysplasia with altered tissue structures as well as an increased number of $CD45^+$ immune cells in comparison with the uninfected control (***Figure 1***, B, C and D). Analysis of the H1N1 injured-lungs of the *ChAT-Cre*: Ai9 mice, which express tdTomato proteins in the ChAT-expressing cells, showed that about 78% ChAT-expressing cells also expressed the tuft cell marker *Dclk1* whereas about 60% and 12% of ChAT-expressing cells expressed the other two taste signaling proteins Gα-gustducin and *Plcβ2*, respectively (***Figure 1***, E and F). In addition, chemically induced severe lung injury with bleomycin, lipopolysaccharide and powder of house dust mite extracts also led to the generation of dysplastic tuft cells, but to a lesser extent (***Figure 1—figure Supplement 1***), confirming the severe injury-induced formation of ectopic tuft cells in the lung parenchyma (***Rane et al. 2019***; ***Barr et al. 2022***; ***Huang et al. 2022***).

Ectopic lung tuft cells respond to bitter tasting compounds

To assess how the severe lung injury may affect the bitter taste receptor expression, we quantified and comparatively analyzed Tas2r expression levels by performing quantitative reverse transcription-PCR on the WT lung tissues before and after H1N1 infection. The results showed that the expression levels of most of murine 35 Tas2rs remained unchanged while *Tas2r105*, *Tas2r108*, *Tas2r118*, *Tas2r137* and *Tas2r138* were upregulated, and *Tas2r135* and *Tas2r143* downregulated (***Figure 2***A), which is largely consistent with the single cell RNAseq data (***Barr et al. 2022***), suggesting that the upregulated Tas2rs are indeed expressed in these ectopic tuft cells.

To determine whether the taste signal transduction pathways present in these ectopic lung tuft cells are functional, we isolated these tuft cells from the *ChAT-Cre*: Ai9 mice at 25 dpi by fluorescence-activated cell sorting (FACs) (***Figure 2—figure Supplement 1***) and assessed their intracellular calcium responses to two common bitter taste substances denatonium benzoate (D.B.) and quinine. It is known that D.B. activates mouse bitter taste receptor Tas2r105 whereas quinine can stimulate multiple Tas2rs, including 3 of the 5 upregulated bitter taste receptors: Tas2r105, Tas2r108 and Tas2r137 (***Lossow et al. 2016***). The results showed that subsets of tuft cells responded to these two compounds by increasing the intracellular calcium contractions. Application of the bitter taste inhibitor allyl isothiocyanate (AITC), G protein β moiety inhibitor gallein or *Plcβ2* inhibitor U73122 was able to completely inhibit these cells' calcium responses to the bitter compounds (***Figure 2***B-K), indicating that the Tas2rs and their downstream signaling proteins are functional in subsets of tuft cells, and may play some physiological roles during the transition from inflammatory response to resolution.

Conditional nullification of the taste signaling protein *Gγ13* exacerbates the H1N1-inflicted disease severity and suppresses ectopic tuft cell expansion

To determine what role the taste signaling proteins may play in the H1N1 infection-triggered lung injury, we inoculated H1N1 to the whole-body *Trpm5* knockout mice (*Trpm5*$^{-/-}$) and the conditional

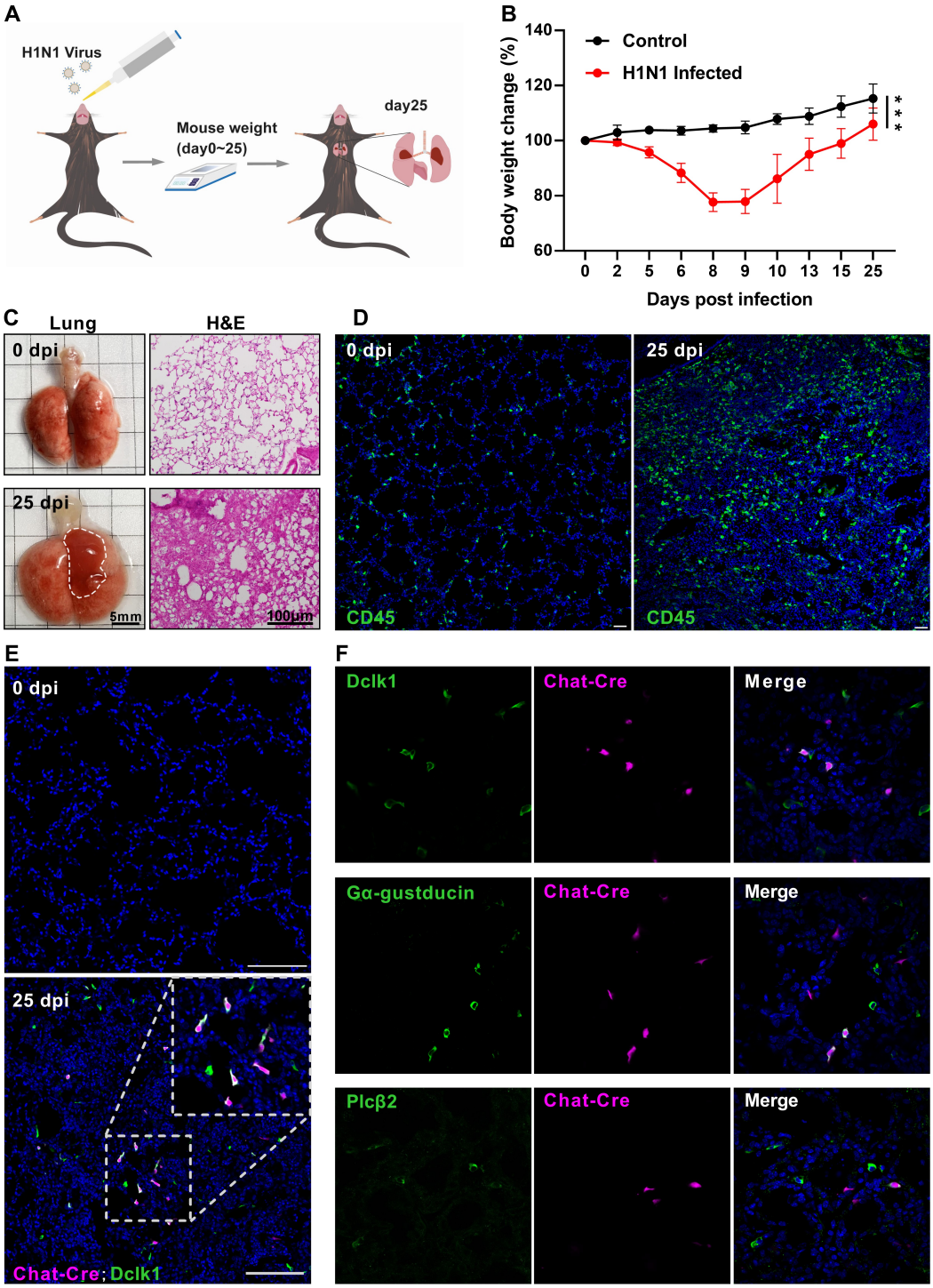

Figure 1. H1N1 infection causes severe damage to mouse lung. (A) Schematic of H1N1 intranasal inoculation procedure. (B) Bodyweight changes of uninfected control and H1N1-infected mice over 25 days post infection. Data are presented as means ± SD (n=6). Unpaired two-tailed student t tests were performed. (C) Representative images of lungs at 0 and 25 dpi, and their H&E tissue sections (Bars: 5 mm in the whole lung images and 100 μm in the lung section images). (D) Immunostaining images of lung sections of 0 and 25 dpi with an antibody to CD45. (E) Immunostaining of the *ChAT-Cre*: Ai9 lung sections of 0 and 25 dpi with the antibody to the tuft cell marker *Dclk1* (green), and ChAT (Ai9, red tdTomato). (F) Immunostaining of the *ChAT-Cre*: Ai9 lung sections of 25 dpi with antibodies to *Dclk1* (green), G*α*-gustducin (green) or *Plcβ2* (green) and ChAT (Ai9, red tdTomato). Scale bars in (D, E, F): 50 μm. ***$P<0.001$.

Figure 1—figure supplement 1. Chemically induced severe injury also engenders ectopic formation of lung tuft cells.

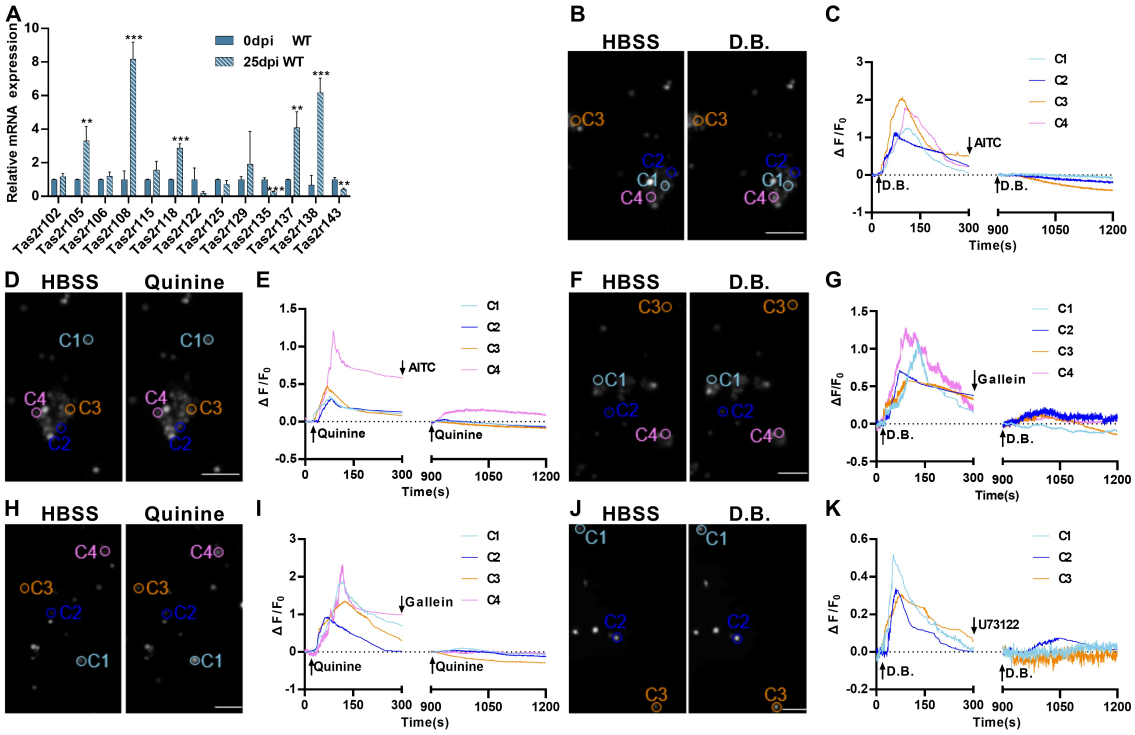

Figure 2. Expression and functional responses of bitter taste receptors. (A) Quantitative RT-PCR analysis of bitter taste receptor expression in the lung tissues at 0 dpi versus 25 dpi. Expression of *Tas2r105*, *Tas2r108*, *Tas2r118*, *Tas2r137* and *Tas2r138* was upregulated whereas *Tas2r135* and *Tas2r143* were downregulated at 25 dpi. Data are presented as means ± SD (n=3). Unpaired two-tailed student t tests were performed. (B-K) Calcium imaging and response traces of FACs-sorted tuft cells isolated from H1N1-infected lungs at 25 dpi. (B, D, F, H, and J) Left panels are grey images of tuft cells at rest in the HBSS buffer whereas right panels are grey images of the same cells after being stimulated by denatonium benzoate (D.B.) or quinine. Activated cells appeared brighter. (C, E, G, I, K) traces of calcium responses of tuft cells on the left. Some tuft cells responded to D.B, which was inhibited by AITC (B, C), gallein (F, G), or U73122 (J, K) whereas others responded to quinine, which was also inhibited by AITC (D, E) or gallein (H, I). Scale bar: 50 μm. ***P*<0.01, ****P*<0.001.

Figure 2—figure supplement 1. FACs sorting of ectopic tuft cells.

Gγ13 knockout mice (*ChAT-Cre: Gng13*$^{flox/flox}$, i.e., *Gng13*-cKO) as well as WT control mice. Results indicated that while WT and *Trpm5*$^{-/-}$ mice showed similar bodyweight loss/recovery curves with nearly no mortality, *Gng13*-cKO mice exhibited significantly more bodyweight loss with a maximum of 30% instead of 20% of the original bodyweight, and a slower recovery process with a shifted maximum bodyweight loss from 9 dpi to 10 dpi, and a significant increase in the mortality rate to 37.5%, the majority of which occurred between 8 and 12 dpi (***Figure 3***, A and B). Furthermore, the H1N1-infected lungs of WT and *Trpm5*$^{-/-}$ mice at 25 dpi displayed similar injured areas whereas those of *Gng13*-cKO showed significantly greater injured areas (***Figure 3***, C and D). And the ratios of wet-to-dry lung masses of both WT and *Gng13*-cKO mice at 25 dpi were significantly greater than their respective ones at 0 dpi whereas the ratio of the *Gng13*-cKO mice at 25 dpi was even greater than that of WT mice at 25 dpi (***Figure 3***E), supporting the notion that *Gng13*-cKO mice experienced severer damage following H1N1 infection comparing with WT control.

To investigate how the abolishment of taste signaling proteins affects the formation of ectopic lung tuft cells in response to H1N1 infection, we performed immunohistochemistry on lung tissue sections, using an anti-krt5 antibody to demarcate H1N1-damaged areas and an anti-Dclk1 antibody to identify tuft cells. We found as early as 14 dpi a small number, i.e., ~6 and ~4 tuft cells per mm^2 of the krt5-expressing tissue area in WT and *Gng13*-cKO lungs, respectively, and no significant differences in the tuft cell density between these two genotypes were found at this time point.

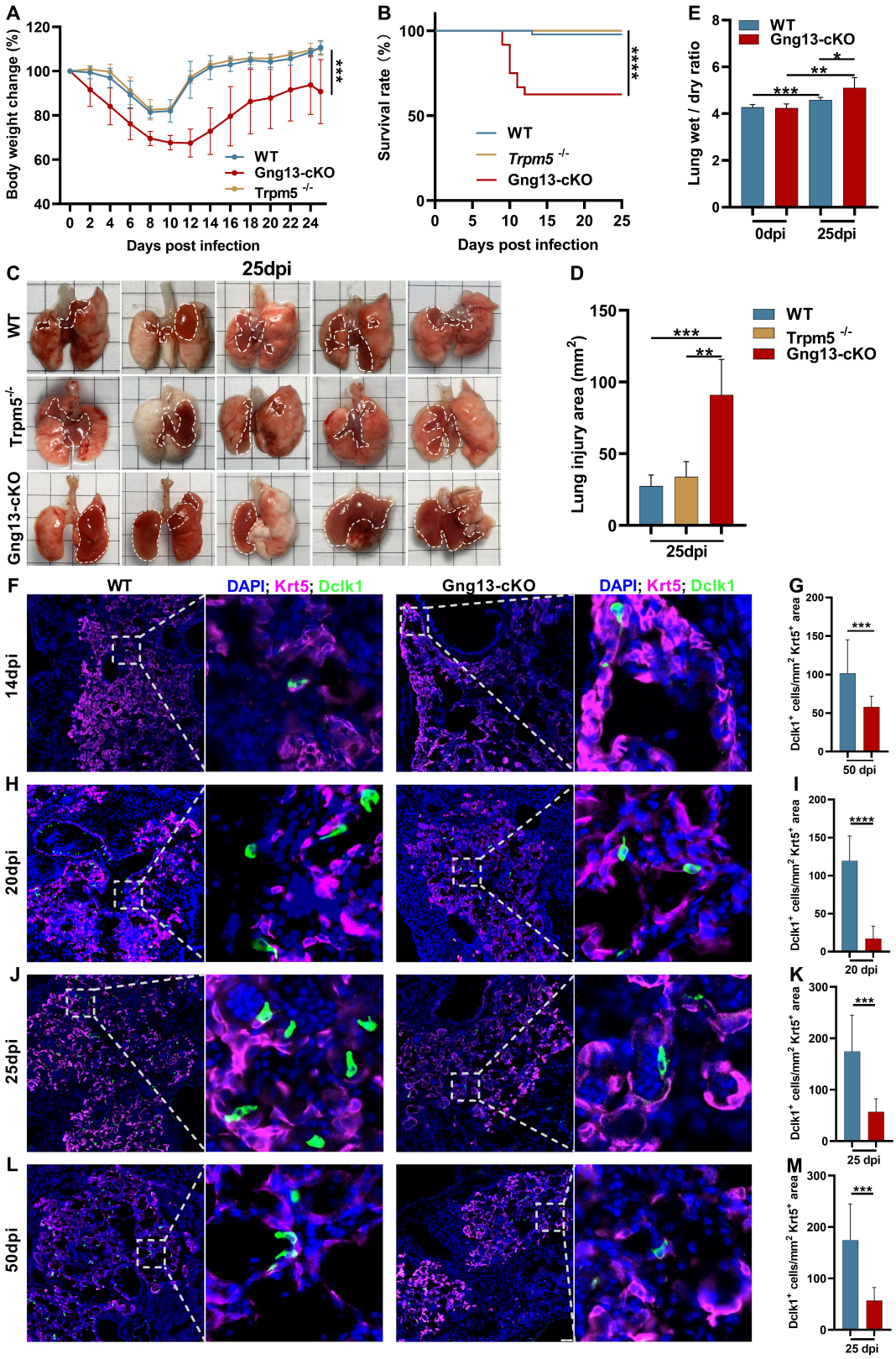

Figure 3. H1N1 infection inflicts differential lung injury and tuft cell dysplasia on WT versus mutant mice. (A) *Gng13*-cKO mice showed

Figure 3 continued on next page

Figure 3 continued
greater bodyweight loss than WT or *Trpm5*$^{-/-}$ mice over days post infection. Data are presented as means ± SD (n=6). Unpaired two-tailed ttests were performed. (B) Kaplan-Meier survival curves of WT, *Trpm5*$^{-/-}$ and *Gng13*-cKO mice following H1N1 inoculation. A significant number of *Gng13*-cKO mice died between 9 and 12 dpi (i.e., 2, 4, 2 mice and 1 mouse died at 9, 10, 11, 12 dpi, respectively), reducing the overall survival rate to 62.5%, significantly lower than those of *Trpm5*$^{-/-}$ or WT mice, of which nearly all survived. Data are presented as means ± SEM (n= 44, 17 and 14 for WT, *Trpm5*$^{-/-}$. and *Gng13*-cKO mice, respectively). The curves were determined by a log-rank test. (C, D) Images and statistical analysis of the injured areas on the lungs of WT, *Trpm5*$^{-/-}$ and *Gng13*-cKO mice at 25 dpi. The injured areas that are marked by dashed lines were significantly greater in the *Gng13*-cKO mice than in *Trpm5*$^{-/-}$ or WT mice while no significant difference was found between the latter two. Data are presented as means ± SD (n=5), and unpaired two-tailed student t tests were performed. (E) Comparative analysis of wet to dry weight ratios of WT and *Gng13*-cKO lungs at 0 and 25 dpi. While no difference in the ratio was found between WT and *Gng13*-cKO mice at 0 dpi, the ratios of these mice at 25 dpi were significantly greater than their corresponding ones at 0 dpi. However, the *Gng13*-cKO ratio was even greater than WT ratio at 25 dpi. Data are presented as means ± SD (n=6), and unpaired two-tailed student t tests were performed. (F-M) Identification of tuft cells in the Krt5-expressing tissue areas of H1N1-injured lungs of WT and *Gng13*-cKO mice at 14, 20, 25 and 50 dpi using antibodies to Krt5 and to the tuft cell marker *Dclk1*. The densities of tuft cells were significantly higher in WT than in *Gng13*-cKO lungs at 20, 25 and 50 dpi, but not at an earlier time point of 14 dpi. Data are presented as means ± SD (n=3), and unpaired two-tailed student t tests were performed. **P*<0.05, ***P*<0.01, ****P*<0.001, *****P*<0.0001.
Figure 3—figure supplement 1. Ectopic generation of tuft cells in WT, *Trpm5*$^{-/-}$ and *Gng13*-cKO mice over days post infection.

However, at 20 and 25 dpi, the densities of tuft cells in WT were increased to 120 and 175 cells per mm^2, respectively, which are significantly more than the corresponding densities of *Gng13*-cKO, i.e., 34 and 57 cells / mm^2, respectively; and at 50 dpi, the tuft cell density in WT was decreased to 102 cells / mm^2, which, however, was still significantly higher than 56 cells / mm^2 of *Gng13*-cKO (***Figure 3***, F-M). In contrast, the densities of tuft cells in *Trpm5*$^{-/-}$ mice were nearly identical to those of WT at both 14 and 25 dpi, and no significant difference was found between WT and *Trpm5*$^{-/-}$ mice (***Figure 3—figure Supplement 1***, A-E). Thus, although tuft cells first appeared at 14 dpi in all WT, *Trpm5*$^{-/-}$ and *Gng13*-cKO mice, and no statistic difference in their densities was found among these mice, the subsequent densities were increased in all WT, *Trpm5*$^{-/-}$ and *Gng13*-cKO mice; and the increase was much less in the *Gng13*-cKO mice than in WT or *Trpm5*$^{-/-}$, and consequently, the densities in the *Gng13*-cKO mice were significantly less than in WT or *Trpm5*$^{-/-}$ mice at 20, 25 and 50 dpi (***Figure 3—figure Supplement 1***F).

To determine how many ectopic tuft cells in the infected WT lung express *Gγ13* and whether any remaining ectopic tuft cells in the infected *Gng13*-cKO lung express *Gγ13*, double immunostaining was carried out with antibodies to *Dclk1* and to *Gγ13* on the lung tissue sections of 25 dpi of both WT and *Gng13*-cKO mice. The results showed that about 28.6% of Dclk1$^+$ ectopic tuft cells express *Gγ13* in WT sections while none of the remaining Dclk1$^+$ tuft cells in the Gng13-cKO sections was *Gγ13*$^+$ (***Figure 3—figure Supplement 1***, G and H), indicating an effective conditional ablation of *Gγ13* expression. This result is consistent with the previous report indicating the heterogeneity of dysplastic tuft cells in the severely injured lung (***Barr et al. 2022***), but a select subset of tuft cells were entirely ablated in this study.

Gγ13 mutant mice display stronger inflammation and augmented pyroptosis following H1N1 infection

To determine whether *Gγ13* conditional knockout affects the inflammation resolution following H1N1 infection, we performed immunohistochemistry on the lung sections with an antibody to the immune cell marker *CD64*. The results showed that at both 20 and 25 dpi, the *Gng13*-cKO mice had significantly more *CD64*$^+$ immune cells in the injured areas than WT, although both types of mice indicated a trend of inflammation resolution with a reduction in the number of immune cells from 20 to 25 dpi (***Figure 4***, A and B).

We also carried out quantitative reverse transcription-PCR (qRT-PCR) to assess the expression of pyroptosis-related gasdermin genes, and found that Gsdmd and Gsdme were the two most abundantly expressed ones (***Figure 4—figure Supplement 1***). Further analysis showed that before H1N1 infection, the expression levels of *Gsdmd* and *Gsdme* were similar between WT and *Gng13*-cKO mice at 0dpi; and at 25 dpi, their expression levels were significantly higher than those at

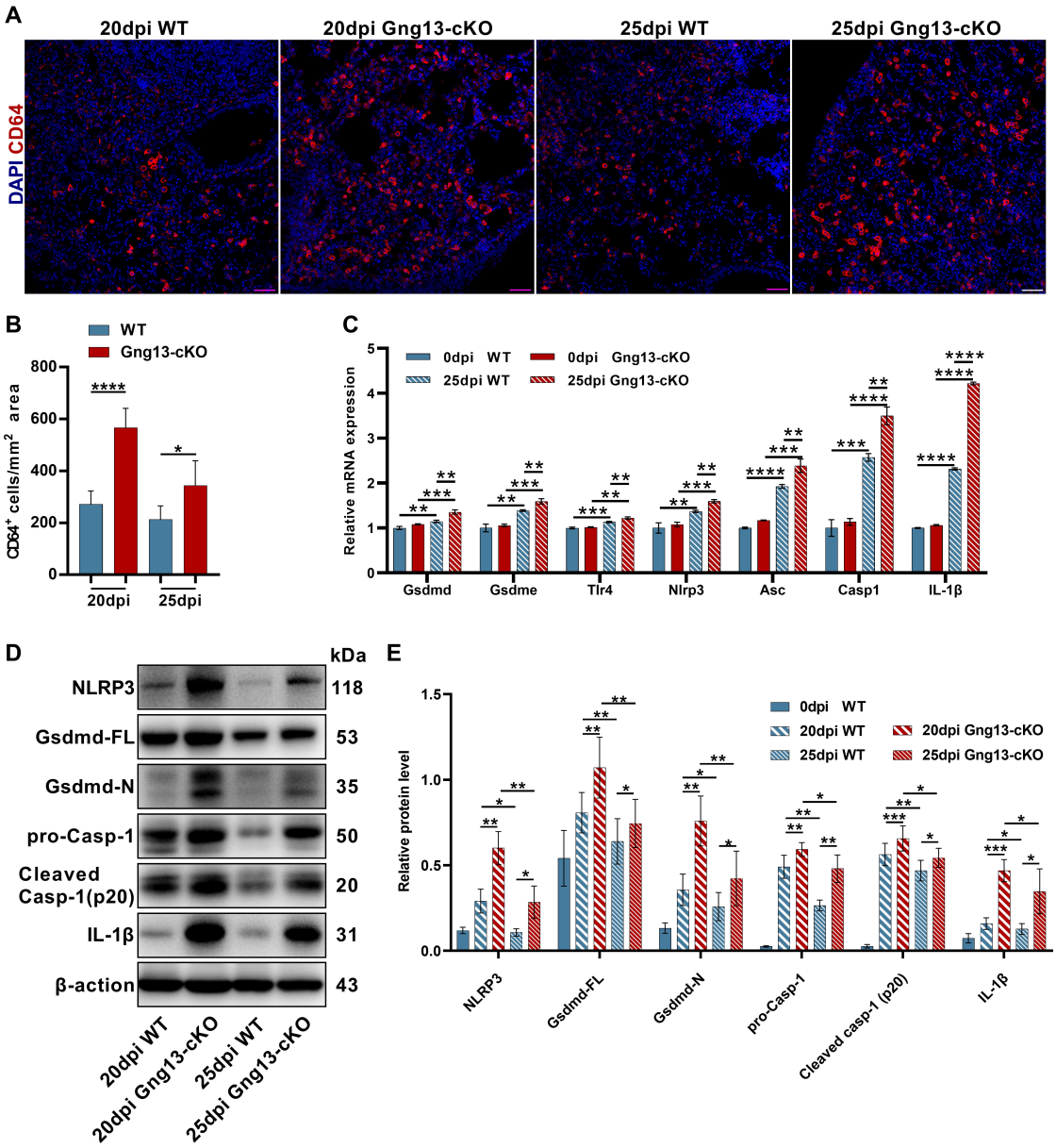

Figure 4. Stronger inflammatory response and upregulated expression of pyroptotic genes in the H1N1-infected *Gng13*-cKO lungs. (A, B) Immunostaining of WT and *Gng13*-cKO lung tissue sections with an antibody to the immune cell marker *CD64* indicates significantly more immune cells in the mutant lung than in WT at both 20 and 25 dpi. (C) qRT-PCR indicates that expression levels of gasdermin D and E (*Gsdmd*, *Gsdme*) and other proteins of the pyroptosis pathway: *Tlr4*, *Nlpr3*, *Asc*, *Casp1* and *Il-1b* were significantly upregulated in both WT and *Gng13*-cKO lungs at 25 dpi comparing with those at 0 dpi. Further, the expression levels of these genes in *Gng13*-cKO were significantly higher than in WT at 25 dpi. Data are presented as means ± SD (n=3). Unpaired two-tailed student t tests were performed. (D, E) Western blot analysis shows that the protein levels of NLRP3, full-length Gasdermin D (*Gsdmd*-FL), N-terminal fragment of Gasdermin D (*Gsdmd*-N), pro-caspase 1 (pro-Casp1), cleaved caspase 1(Cleaved Casp-1 (p20)), and *IL-1β* in the *Gng13*-cKO lungs were significantly higher than the corresponding levels of WT at both 20 and 25 dpi (*β*-actin as an internal control). And over this phase, the expression levels of these proteins were reduced at 25 dpi in comparison with those at 20 dpi in both genotypes. Data are presented as means ± SD (n=4), and unpaired two-tailed t tests were performed. *$P<0.05$, **$P<0.01$, ***$P<0.001$, ****$P<0.0001$.

Figure 4—figure supplement 1. qRT-PCR analysis of gasdermin gene expression in WT and *Gng13*-cKO lungs.

0 dpi in both WT and *Gng13*-cKO mice; furthermore, *Gsdmd* and *Gsdme* expression levels were significantly higher in the *Gng13*-cKO mice than in WT at 25 dpi (***Figure 4***C). We then performed additional qRT-PCR to examine the expression patterns of other genes involved in the pyroptosis, *Tlr4*, *Nlpr3*, *Asc*, *Casp1* and *Il-1b*, and found a similar pattern for all these genes, i.e., both WT and *Gng13*-cKO mice showed more expression at 25 dpi than at 0 dpi, whereas *Gng13*-cKO exhibited even higher expression levels than WT at 25 dpi (***Figure 4***C).

To validate their expression at the protein level, we isolated proteins from the injured lung areas and performed Western blot analysis with antibodies to NLRP3, full-length Gsdmd, N-terminal fragment of Gsdmd, pro-Casp-1, cleaved Casp-1, IL-1β and β-actin as an internal reference (***Figure 4***D). Quantitative analysis showed that at both 20 and 25 dpi, the protein levels of all these pyroptosis pathway proteins were greater in the *Gng13*-cKO mice than in WT mice, and comparison within the same genotype showed that the levels of these proteins at 20 dpi were higher than at 25 dpi in both WT and *Gng13*-cKO mice (***Figure 4***E).

To determine which cells underwent pyroptosis, we performed immunohistochemistry on the injured lung sections with antibodies to the two most highly expressed gasdermins, *Gsdmd* and *Gsdme*. Results showed that at 25 dpi, there were about 180 and 77 cells/mm^2 in *Gng13*-cKO mice expressing *Gsdmd* and *Gsdme*, respectively, which are significantly higher than the corresponding densities of 88 and 50 in WT (***Figure 5***, A and B; ***Figure 5—figure Supplement 1***, A and B). Colocalization of immunostaining with antibodies to *Gsdmd*, the macrophage marker F4/80 and the epithelial cell marker EpCAM, indicated that the majority of Gsdmd$^+$ cells, i.e., about 76.7% and 80.6% in WT and *Gng13*-cKO mice, respectively, at 25 dpi were also F4/80$^+$, and the remaining Gsdmd$^+$ cells, i.e. 21.9% and 17.8% of Gsdmd$^+$ cells in WT and *Gng13*-cKO mice, respectively, were *EpCAM*$^+$, suggesting that most of Gsdmd-expressing cells were macrophages whereas the remaining were epithelial cells (***Figure 5*** C, ***Figure 5—figure Supplement 2***A). Interestingly, nearly all (i.e., 98.5% and 95.5% in WT and *Gng13*-cKO, respectively) of Gsdme$^+$ cells were F4/80$^+$, indicating that almost all Gsdme-expressing cells were macrophages in the two genotypes at 25 dpi (***Figure 5—figure Supplement 2***B). Finally, the density of cells expressing *IL-1β* and caspase 3 were 153 cells/mm^2 and 267 cells/mm^2, respectively, in *Gng13*-cKO mice at 25 dpi, and significantly greater than the corresponding density of 63 and 66 cells/ mm^2 in WT mice (***Figure 5***, D and E; ***Figure 5—figure Supplement 1***, C and D), indicating more programmed cell death in the H1N1-infected *Gng13*-cKO lung. Similar to that of *Gsdme*, the majority, i.e., 9% and 91%, of IL-1β-expressing cells in WT and *Gng13*-cKO mice, respectively, were F4/80$^+$ macrophages (***Figure 5—figure Supplement 2***C).

To obtain a snapshot of cells indeed undergoing pyroptosis, we intranasally administrated Sytox to label pyroptotic cells. Histochemical analysis showed that *Gng13*-cKO mice at 20 and 25 dpi had 211 and 96 Sytox$^+$ cells/mm^2, respectively, significantly more than the corresponding 96 and 62 cells/mm^2 in WT (***Figure 6***, A and B). Double staining of Sytox with an anti-CD64 antibody indicated that more than half of *CD64*$^+$ macrophages, i.e., 61.5% and 57% in WT and *Gng13*-cKO mice at 25 dpi, respectively, were *Sytox*$^+$, undergoing pyroptosis (***Figure 6***C). Together, these data indicate that the injured lungs exhibited immune cell infiltration, expressed pyroptotic genes, and cell death of macrophages and some epithelial cells; and from 20 to 25 dpi, the injured animals showed some inflammation resolution; but at both time points, the *Gng13*-cKO mice showed stronger inflammatory responses and slower inflammation resolution than WT.

Gγ13 disruption leads to severer leakage of the lung epithelia

Increased pyroptosis in the mutant lungs prompted us to assess the integrity of lung epithelia. We collected total bronchoalveolar lavage fluid (BALF) from both WT and *Gng13*-cKO mice at both 0, 20 and 25 dpi, and the average numbers of cells per mouse present in the BALF from WT and *Gng13*-cKO mice at 0 dpi were determined to be 0.23x10^6 and 0.37x10^6 cells, respectively, and no significant difference was found between these BALF samples. However, the cell numbers were significantly increased to 1.22 x10^6 and 5.19 x10^6 in WT and *Gng13*-cKO BALF at 20 dpi, and 0.93 x10^6 and 2.63 x10^6 in WT and *Gng13*-cKO BALF at 25 dpi, respectively, and the latter was still significantly

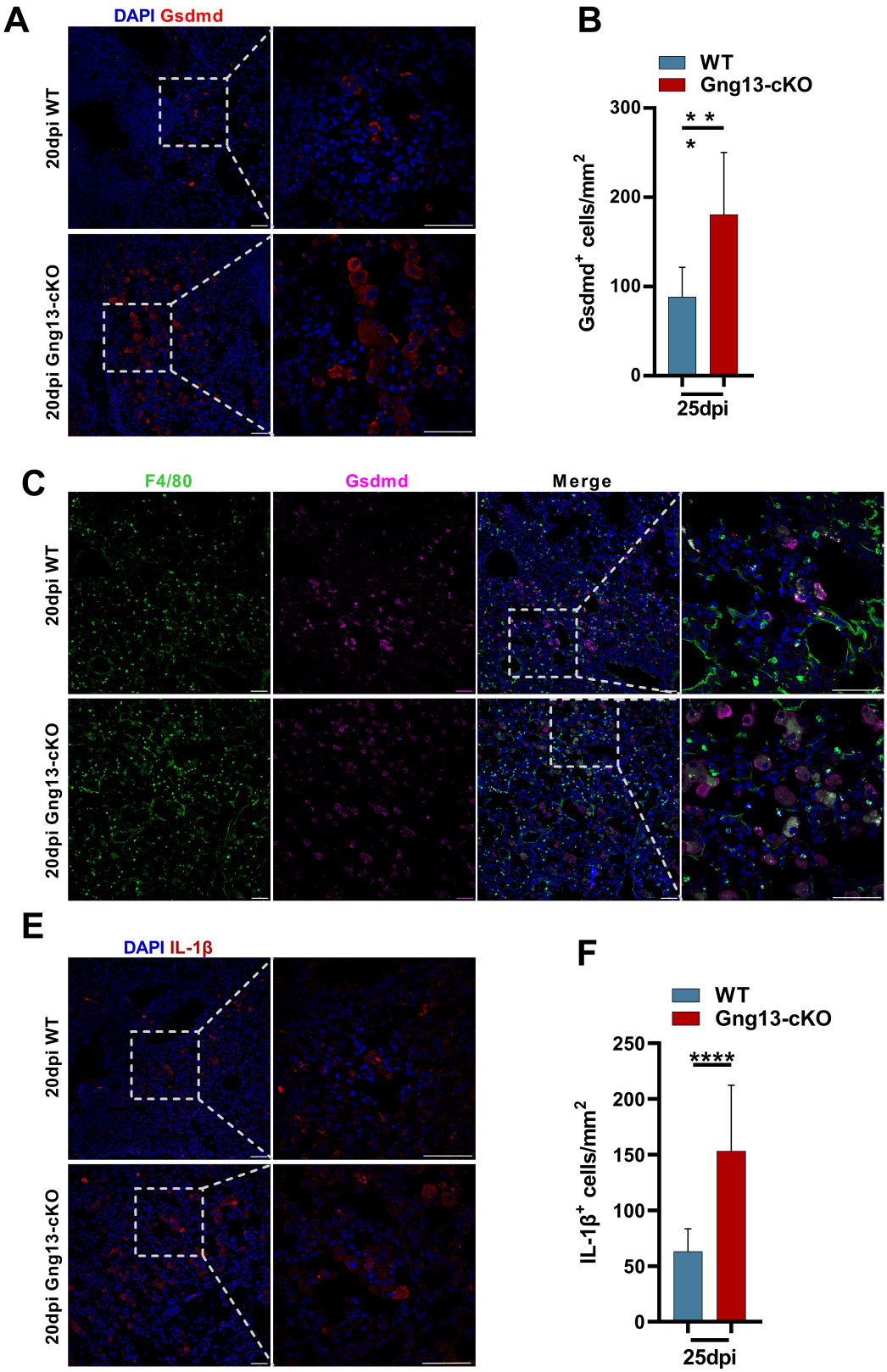

Figure 5. Immunohistochemical analyses of gasdermin D and IL-1β expressing cells. (A, B) Immunostaining of H1N1-infected lung sections

Figure 5 continued on next page

Figure 5 continued
at 25 dpi with an antibody to gasdermin D (*Gsdmd*) indicates significantly more gasdermin D-expressing cells in the *Gng13*-cKO sections than in WT. Data are presented as means ± SD (n=3), and unpaired two-tailed student t tests were performed. (C) Co-immunostaining shows that nearly the same percentage, i.e., 98.5% and 95.5% of Gsdmd$^+$ cells in WT and *Gng13*-cKO, respectively, were F4/80$^+$. (D) Immunostaining of H1N1-infected lung sections at 25 dpi with an antibody to *IL-1β* indicates significantly more IL-1*β*-expressing cells in the *Gng13*-cKO sections than in WT. Data are presented as means ± SD (n=4), and unpaired two-tailed t tests were performed. ***P<0.001, ****P<0.0001.
Figure 5—figure supplement 1. Expression of gasdermin E and caspase 3 in the H1N1-injured lungs.
Figure 5—figure supplement 2. Partial colocalization of gasdermin D, E and *IL-1β* to epithelial cells and macrophages.

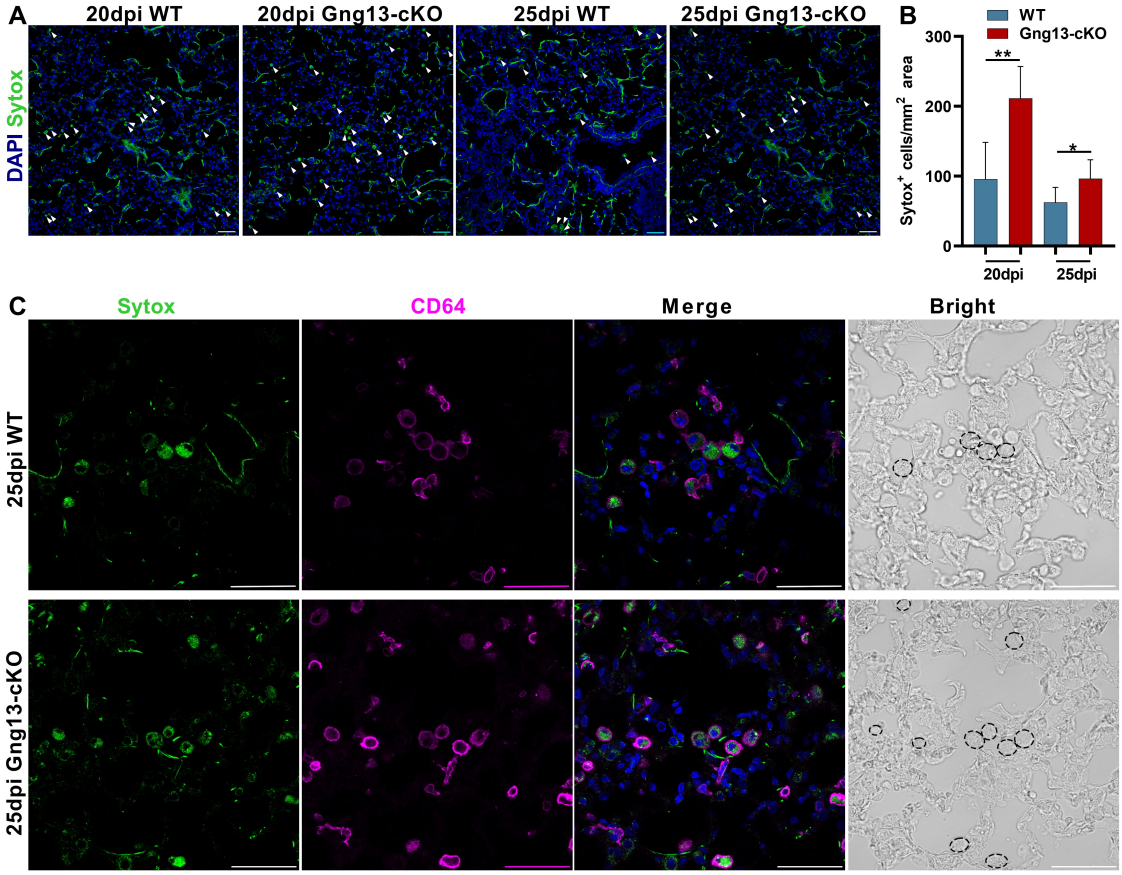

Figure 6. Gng13 conditional nullification leads to more pyroptotic cells in the injured lungs. (A, B) Histological analysis of lung tissue sections following Sytox administration reveals that significantly more Sytox$^+$ cells were found in the mutant lung sections than the corresponding WT tissues at both 20 and 25 dpi while in both types of mice the numbers of the Sytox$^+$ cells at 25 dpi seemed to be fewer than at 20 dpi. (C) Immunostaining with an antibody to the macrophage marker *CD64* indicates that most of Sytox$^+$ cells were macrophages in both WT and *Gng13*-cKO mice (circled by dashed lines in the bright field images on the far right). Data are presented as means ± SD (n=3), and unpaired two-tailed student t tests were performed. *P<0.05, **P<0.01.

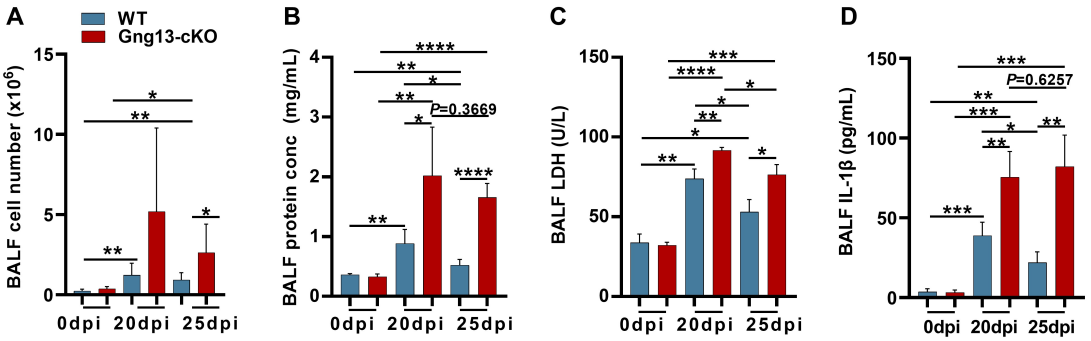

Figure 7. Bronchoalveolar lavage fluid (BALF) assays. (A) Average numbers of cells per mouse found in both WT and *Gng13*-cKO BALFs at 25 dpi were significantly more than those at 0 dpi while those of the *Gng13*-cKO BALF at 25 dpi were even more than those of WT at 25 dpi. Data are presented as means ± SD (n=6), and unpaired two-tailed student t tests were performed. (B) The protein contents of both WT BALF and *Gng13*-cKO BALF at 20 dpi and 25 dpi were significantly more than their corresponding ones at 0 dpi, but the *Gng13*-cKO BALF had significantly more proteins than WT at both 20 and 25 dpi. And in WT, the protein content was significantly reduced from 20 dpi to 25 dpi, but the reduction in the *Gng13*-cKO was insignificant. Data are presented as means ± SD (n=5), and unpaired two-tailed student t tests were performed. (C) Lactate dehydrogenase (LDH) activity assays showed that at both 20 and 25 dpi, LDH activities in both WT and *Gng13*-cKO BALF were significantly higher than their corresponding ones at 0 dpi, but the *Gng13*-cKO BALF at both 20 and 25 dpi showed higher activities than the corresponding WT BALF. And both WT and *Gng13*-cKO BALF displayed significant LDH activity reduction from 20 to 25 dpi. Data are presented as means ± SD (n=3), and unpaired two-tailed student t tests were performed. (D) *IL-1β* ELISA assays showed a similar patter to that of LDH, except that the reduction in the *IL-1β* concentration from 20 to 25 dpi was insignificant in the *Gng13*-cKO BALF. Data are presented as means ± SD (n=4), and unpaired two-tailed student t tests were performed. *P<0.05, **P<0.01.

more than the former (***Figure 7***A). The BALF protein content also showed a similar pattern, i.e., a basal amount of protein was found in both WT and *Gng13*-cKO BALF at 0 dpi, that is, 0.36 and 0.33 mg/mL, respectively, and no significant difference was found between the two groups. At 20 dpi, however, both WT and *Gng13*-cKO BALF contained much more proteins than their corresponding samples at 0 dpi, but the *Gng13*-cKO BALF had more proteins than that of WT (2.01 versus 0.88 mg/mL), and the same is true at 25 dpi (1.65 versus 0.52 mg/mL) (***Figure 7***B). In WT, the BALF protein concentration was significantly decreased from 0.88 mg/mL at 20 dpi to 0.52 mg/mL at 25 dpi whereas the decrease of the BALF protein concentration in the *Gng13*-cKO was insignificant over the same period. The lactate dehydrogenase (LDH) activity and *IL-1β* content in the BALF also showed similar patterns. No significant difference in the basal LDH activity or *IL-1β* content was found between WT BALF (LDH, 33.81 U/L; *IL-1β*, 3.60 pg/ml) and *Gng13*-cKO BALF (LDH, 32.17 U/L; *IL-1β*, 3.35 pg/ml) at 0 dpi. The LDH activity then rose significantly to 73.86 U/L and 91.67 U/L at 20 dpi in WT and *Gng13*-cKO BALF, respectively, followed by a significant decrease to 53.12 U/L and 76.40 U/L, respectively, at 25 dpi. However, at both time points, the *Gng13*-cKO LDH activities were always greater than the corresponding WT activities (***Figure 7***C). WT BALF *IL-1β* content also significantly increased to 38.82 pg/ml at 20 dpi, then significantly decreased to 22.03 pg/ml at 25 dpi, while the *Gng13*-cKO BALF *IL-1β* levels at the two time points were 75.57 and 82.12 pg/ml, respectively, significantly higher than the corresponding WT levels. Interestingly, different from the LDH activity dynamics, the *Gng13*-cKO BALF *IL-1β* level at 25 dpi did not appear to be reduced comparing with that at 20 dpi (***Figure 7***D). These results indicate that while the WT injured lungs showed significant improvements in the epithelial leakage from 20 to 25 dpi, the *Gng13*-cKO injured lungs displayed higher levels of leakage and a slower repair with a significant reduction only in the BALF LDH level, but not in the total BALF protein or *IL-1β* level, from 20 to 25 dpi.

Gng13 conditional nullification exacerbates H1N1-induced fibrosis

To assay how the *Gng13* mutation affects the recovery of the severely injured lungs, we first conducted qRT-PCR to determine the expression levels of fibrotic genes: *Col1a1*, *Fn1* and *Timp1*. The

results showed that at 0 dpi, there was no significantly difference in the expression levels of these three genes between WT and *Gng13*-cKO lungs; and at 25 dpi, however, the expression levels of these genes were significantly increased in both genotypes comparing with their corresponding levels at 0dpi. Comparison between the two genotypes revealed that at 25 dpi, the expression levels of all these three genes were significantly higher in the *Gng13*-cKO lungs than in WT. At 50 dpi, the expression levels of these genes showed a downward trend in both WT and *Gng13*-cKO lungs, consistent with the phase of return to homeostasis of the remodeled lungs. More specifically, the *Col1a1* expression was reduced to a similar level in WT and *Gng13*-cKO, but still significantly higher than those at 0 dpi. For *Fn1* and *Timp1*, their expression in WT at 50 dpi was much reduced, to a level similar to those at 0 dpi; and their expression in *Gng13*-cKO at 50 dpi was reduced comparing with that at 25 dpi, but still higher than that at 0 dpi or in WT at 50 dpi (***Figure 8***A).

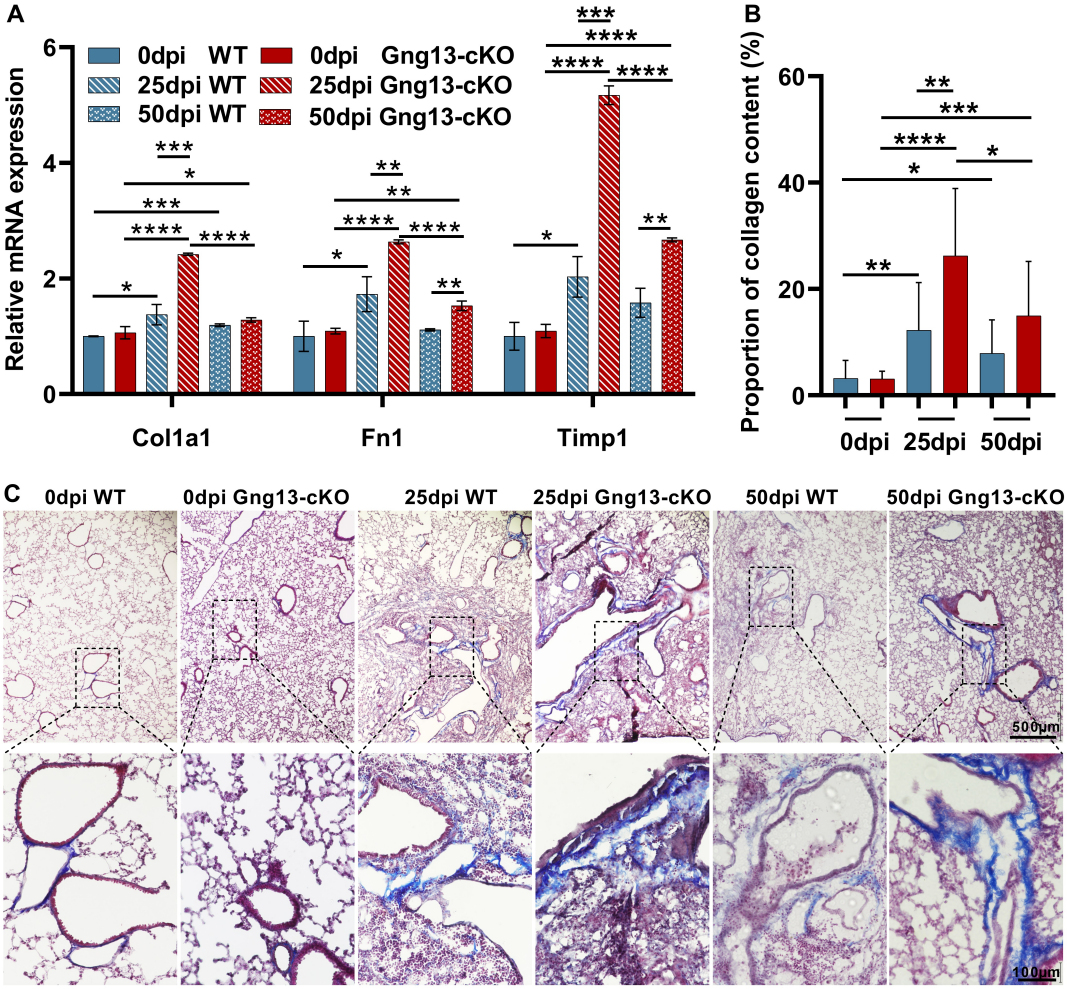

Figure 8. More severe fibrosis in the H1N1-infected *Gng13*-cKO lungs. (A) qRT-PCR analysis of Col1a1, Fn1 and Timp1 expression. While the expression levels of these three genes at 20 dpi in both WT and *Gng13*-cKO injured lungs were significantly greater than their corresponding ones at 0 dpi, the expression in the *Gng13*-cKO at 25 dpi was much stronger than WT at 25 dpi. At 50 dpi, the expression levels of all these three genes were reduced comparing with those at 25 dpi in both WT and *Gng13*-cKO mice, but those of Fn1 and Timp1 in *Gng13*-cKO mice at 50 dpi were still significantly higher than WT at 50 dpi. Data are presented as means ± SD (n=3), and unpaired two-tailed student t tests were performed. (B, C) Masson's trichrome staining showed that at 25 dpi, the fibrosis percentages in WT and *Gng13*-cKO were significantly more than their corresponding ones at 0 dpi, which were reduced at 50 dpi. Data are presented as means ± SD (n=3), and unpaired two-tailed student t tests were performed. *P<0.05, **P<0.01, ***P<0.001, ****P<0.0001.

Masson's trichrome staining was used to determine the extent of fibrosis. The results showed that 3.2% and 3.1% of fibrosis areas were found in WT and *Gng13*-cKO lungs at 0 dpi, respectively, and no significant difference was found between these two genotypes. At 25 dpi, the percentages of fibrosis areas in WT (12.3%) and *Gng13*-cKO (26.3%) were significantly more than their corresponding ones at 0 dpi. And between the two genotypes, the fibrosis in *Gng13*-cKO was even more than that in WT at 25 dpi. At 50 dpi, the fibrosis in WT (7.9%) and *Gng13*-cKO (15%) appeared to be reduced comparing with those at 25 dpi, but they were still more than those at 0 dpi; and furthermore, fibrosis in *Gng13*-cKO at 50 dpi seemed to be more than that of WT at 50 dpi (***Figure 8*** B and C). These results indicate that *Gng13*-cKO mice recovered not as fast as WT mice and displayed a higher level of fibrosis.

Discussion

Multiple subtypes of tuft cells have been found in various organs, but their distinct functions are not well understood. In this study, we used a conditional gene knockout mouse strain to nullify *Gγ13* expression in the ChAT-expressing tuft cells, and found that the number of ectopic tuft cells was reduced in the H1N1 virus-injured lung areas, and all of these remaining tuft cells were *Gγ13*-negative. Furthermore, the *Gng13*-cKO mice displayed larger injured areas in the infected lungs, along with heavier immune cell infiltration, severer and prolonged inflammation, increased pyroptosis and cell death, exacerbated lung epithelial leakage and aggravated fibrosis, increased bodyweight loss and heightened fatality. These results imply that the subsets of *Gγ13*-positive versus negative ectopic tuft cells may play opposite but perhaps balanced roles in the inflammation resolution, tissue repair and functional recovery, and the absence of *Gγ13*-positive tuft cells engenders (***Huang et al. 1999***; ***Wong et al. 1996***; ***Tizzano et al. 2008***), phospholipase C*β*2 (*Plcβ2*) and *Trpm5*. Tuft cells can be deemed as hyper inflammation, consequently leading to aggravated outcomes.

Many signaling proteins are shared by tuft cells and taste receptor cells, including the G protein-coupled Tas1r and Tas2r receptors (***Zhao et al. 2003***; ***Max et al. 2001***; ***Matsunami et al. 2000***; ***Chandrashekar et al. 2000***; ***Adler et al. 2000***), the heterotrimeric G proteins subunits G*α*-gustducin, G*α*14, G*β*1, G*β*3 and G*γ*13 solitary chemosensory cells that are dispersed over many organs of the body, monitoring internal environments, whereas taste receptor cells are aggregated into specialized end organs of taste, taste buds, located in the oral cavity of mammals, evaluating food's nutritional value or potential toxicity before ingestion (***Lindemann 1996***;***O'Leary et al. 2019***). However, there are some important differences between taste buds and tuft cells. For example, distinct subsets of taste bud cells express Tas1rs and Tas2rs, which are employed to detect high-energy carbohydrates, nutritious amino acids, or potentially harmful and toxic substances, respectively, conveying the chemical information via different gustatory nerve fibers to the central nervous system, generating hedonic sweet and umami taste perception or unpleasant bitter taste (***Doyle et al. 2023***). In contrast, individual tuft cells can express both Tas1rs and Tas2rs, and the latter are indeed also involved in the detection of infectious microbes and invading parasites that pose risks to the host's health whereas the function of the former is less clear, and seems to regulate Tas2rs' signaling or tuft cell homeostasis (***Howitt et al. 2020***). Results of our present study indicate that Tas2rs expressed by the ectopic tuft cells are also functional, and could be involved in monitoring changes in the extracellular milieu of the injured areas during the switch from the inflammatory response to inflammation resolution, regulating disease progression.

Our results show that ectopic tuft cells first appear around days 12 to 14 post influenza infection and then the tuft cell number increases over the next two months, which is consistent with previous report (***Rane et al. 2019***). However, our study further indicates that the conditional knockout of *Gng13* in the ChAT-expressing tuft cells did not affect the generation of dysplastic tuft cells up to 14 days post H1N1 infection, but did decrease ectopic tuft cells' capability to expand at 20 dpi or later, suggesting that different molecular mechanisms are employed for the initial generation versus subsequent expansion of these tuft cells: the former does not require the contribution from *Gγ13*-mediated signal transduction whereas the latter does require positive feedback signals

released by *Gγ13*-mediated signaling pathways. It is still unclear how chemically or virally induced major injuries generate these dysplastic tuft cells in the distal lung tissues. Severe injuries can activate quiescent lineage-negative stem/progenitor cells in the pulmonary epithelia via a Notch signaling pathway to proliferate and differentiate into different types of pulmonary epithelial cells to repair and remodel the wounded tissues (**Rane et al. 2019**; **Vaughan et al. 2015**). But the exact signals that activate the quiescent stem cells are yet to be identified, although these signals can presumably originate from the apoptotic cells or activated immune cells following the chemical injuries or viral infection. Once activated, the stem/progenitor cells express the transcription factor *Pou2f3* at a cell-type specification stage, which has been shown to be critical to the formation of both tuft cells throughout the body and Tas1r- and Tas2r-expressing receptor cells in taste buds, as nullification of the *Pou2f3* gene ablates all these taste receptor cells and tuft cells (**Gerbe et al. 2016**; **Matsumoto et al. 2011**; **Ualiyeva et al. 2020**; **Yamashita et al. 2017**). *Pou2f3* may interact with other accessory proteins such as POU domain class 2 associating factors 2 and 3, i.e., *Pou2af2* and *Pou2af3*, respectively, to fine-tune gene expression patterns and direct these cells to differentiate into subtypes of tuft cells or taste receptor cells (**Wu et al. 2022**). On the other hand, a negative regulatory mechanism has been reported, suggesting that the activating transcription factor 5 (*ATF5*) appears to inhibit the generation of intestinal tuft cells since more tuft cells were found in the ATF5-deficient ileum (**Nakano et al. 2023**). Presumably, some intrinsic and extrinsic factors from the severely damaged lung tissues may regulate the activation of Notch, *Pou2f3* and *ATF5*, and together with additional transcription factors such as Gfi1b and Spdef, control the generation of subtypes of ectopic tuft cells in the injured lung.

The proliferation of intestinal tuft cells is dependent on *Trpm5* (**Howitt et al. 2016**; **Lei et al. 2018**; **Luo et al. 2019**), but the tracheal tuft cells or sweet, umami and bitter taste receptor cells in taste buds do not require *Trpm5* for their expansion (**Damak et al. 2006**; **Zhang et al. 2003**; **Finger et al. 2005**; **Hollenhorst et al. 2022**). We and others have found that *Trpm5* is not required for the proliferation of the dysplastic pulmonary tuft cells (**Barr et al. 2022**; **Huang et al. 2022**), but conditional nullification of Gng13 ablated part of these ectopic tuft cells and reduced the total number of these cells, indicating that different tuft cells utilize different mechanisms to control their proliferation. In the small intestine, the hyperplasia of tuft cells as well as goblet cells is regulated by the *Trpm5- IL25- ILC2- IL13* molecular circuit. Pathogens or microbial metabolites activate the succinate receptor Sucnr1, Tas2rs, Vmn2r26 and prostaglandin receptors and possibly other GPCRs, which then stimulate the heterotrimeric G proteins composed of Gα-gustducin, Gβ1, Gβ3, and Gγ13. Single-cell RNAseq data have shown that many of these GPCRs and G protein subunits are co-expressed in the intestinal as well as ectopic pulmonary tuft cells although additional G protein subunits could also be involved in the signal transduction (**Barr et al., 2022**). Upon activation, the heterotrimeric G$\alpha\beta\gamma$ dissociates into the Gα and G$\beta\gamma$13 moieties, each of which can act on their own effectors. While Gα-gustducin's effectors are still to be determined, G$\beta\gamma$13 can act on the phospholipase *Plcβ2* or other effectors such as adenylate cyclases, phospholipases, receptor kinases, voltage-gated ion channels and inward rectifying ion channels (**Campbell and Smrcka 2018**; **Kankanamge et al. 2022**). Among them, *Plcβ2* can generate the second messengers diacylglycerol (DAG) and inositol trisphosphate (IP3) (**Huang et al. 1999**). DAG can activate a number of protein kinases, but their eventual physiological effect is yet to be elucidated. On the other hand, IP3 can bind to and open its channel receptor IP3R on the endoplasmic reticulum (ER), releasing the calcium ions from the ER and consequently increasing the cytosolic calcium concentration, leading to the opening of *Trpm5*, a calcium-activated non-selective monovalent cation channel, depolarizing the membrane potential and releasing certain output signals (**Zhang et al. 2007**; **Liman 2014**). The release of the cytokine IL-25, acetylcholine (ACh), ATP, calcitonin gene-related peptide (CGRP) and component C3 from tuft cells and taste bud cells is dependent on *Trpm5*, but that of some antimicrobial substance and eicosanoids does not require *Trpm5* (**Lee et al. 2014**), indicating that *Trpm5* regulates only some output signals' release. Since the expansion of ectopic tuft cells is independent of *Trpm5*, we believe that *Trpm5*-dependent output signaling molecules may not be involved in the regulation of

these tuft cells' proliferation. On the other hand, the elimination of *Gγ13*-expressing pulmonary tuft cells in the *Gng13*-cKO mice suggests that the effectors activated by the G$\beta\gamma$13 moiety are involved in the regulation of output signals that promote the proliferation of *Gγ13*-expressing tuft cells. The differential impact of *Trpm5* knockout versus Gng13 abolishment on tuft cell proliferation is probably attributed to the fact that *Gγ13* is upstream of *Trpm5* in the signaling cascades, thus regulating more signaling pathways, and when mutated, having a more profound effect than *Trpm5*. Further investigation is needed to determine what signals the *Gγ13*-positive and -negative ectopic pulmonary tuft cells are needed to expand, and with this knowledge, one could intentionally manipulate increasing the clinically beneficial subtypes while decreasing the harmful ones of dysplastic tuft cells.

Previous reports indicate that elimination of all ectopic tuft cells by knocking out the *Pou2f3* gene did not significantly affect the pathogenesis and outcome of H1N1-induced severe injury (***Barr et al. 2022***;***Huang et al. 2022***). In our study, elimination of *Gγ13*-expressing ectopic pulmonary tuft cells rendered severer symptoms following H1N1 infection, ranging from more immune cell infiltration, increased pyroptotic gene expression and cell death, larger injury areas in the lungs, more BALF protein contents and immune cells, and larger areas of fibrosis, to a slower recovery process and higher fatality rate. The striking discrepancy may be caused by the imbalance of tuft cells' diverse functions in the *Gng13*-cKO lung. Since the ectopic tuft cells are absent until 12-14 dpi, these cells may not be involved in the initial inflammatory responses to viral infection or the subsequent viral clearance. When the pathogeneses enter the later stages, the *Gng13*-cKO lungs have a much reduced number of tuft cells with only a few of *Gγ13*-negative tuft cells remaining, leading to much severer symptoms, indicating that the missing tuft cells may play a major role in the transition from the inflammatory responses to inflammation resolution and subsequent tissue repair processes while the remaining tuft cells are unable to effectively contribute to these processes, or even worse, stimulate inflammation.

Indeed, some tuft cells have been shown to produce pro-inflammatory cytokines and lipid mediators such as IL-25, prostaglandins and leukotrienes that activate innate and adaptive immune responses (***Kotas et al. 2022***; ***Ualiyeva et al. 2021***; ***Hollenhorst and Krasteva-Christ 2023***), and single cell RNAseq analyses indicate that pulmonary ectopic tuft cells express genes that encode enzymes producing specialized pro-resolving mediators (SPMs), for example, *Alox5*, *Alox12e*, *Alox15*, *Ptgs2*, encoding arachidonate 5-lipoxygenase (5-LOX), arachidonate 12-lipoxygenase (12-LOX), arachidonate 15-lipoxygenase (15-LOX), prostaglandin-endoperoxide synthase II (also known as cyclooxygenase II, COX-2), respectively, as well as the genes encoding various isoforms of cytochrome P450: *Cyp51*, *Cyp2f2*, *Cyp7b1* and *Cyp2j6* (***Barr et al. 2022***). These enzymes can utilize membrane lipids such as docosahexaenoid acid, eicosapentaenoid acid and arachidonic acid to biosynthesize SPMs, including lipoxins, resolvins, protectins, and maresins, which can limit further infiltration of neutrophils, recruit and stimulate macrophage phagocytosis to remove dead cells and cell debris, suppress the production of pro-inflammatory mediators and cytokines, and increase the production of anti-inflammatory mediators and cytokines, reduce fibrosis and accelerate tissue repair and remodeling (***Serhan et al. 2020***; ***Panigrahy et al. 2021***). So far, the SPMs maresin 1 and resolvin D1 have been shown to inhibit virus- and bacterium-induced inflammation in the lung, respectively (***Krishnamoorthy et al. 2023***; ***Codagnone et al. 2018***). Together, our data from this study imply that nullification of Gng13 not only significantly reduces the number of ectopic tuft cells but also disrupts the switch from producing proinflammatory lipid mediators to producing anti-inflammatory SPMs. Given the heterogeneity of tuft cells (***Xiong et al. 2022***; ***Bankova et al. 2018***; ***Haber et al. 2017***), we hypothesize that the remaining dysplastic tuft cells may continue to produce proinflammatory cytokines and lipid mediators whereas the anti-inflammatory agents-producing tuft cells are absent in the *Gng13*-cKO mice, consequently leading to severer outcomes.

In conclusion, to our knowledge, it is first time to pustulate that different subtype of tuft cells may play different subtype-specific roles at the phases of infection, response, resolution, and recovery upon H1N1 infection or other severe injuries. Our data reveal that *Gγ13*-expressing ectopic

tuft cells promote the inflammation resolution and recovery while other dysplastic lung tuft cells contribute to extended inflammation and perhaps immune storms as well.

Methods and Materials

Experimental design

This study was designed to investigate the possible roles of the taste signaling proteins, the heterotrimeric G protein subunit Gγ13 and the transient receptor potential ion channel Trpm5, in the host response to H1N1 influenza virus infection as well as in the subsequent inflammation resolution, tissue remodeling and recovery using transgenic and conditional gene knockout mouse models with wild-type (WT) mice as control. Animals were intranasally inoculated with H1N1 viruses at a sublethal dosage, their bodyweights were measured, mortality rates determined; the lung tissues and bronchoalveolar lavage fluid were molecularly, biochemically, immunologically, and statistically analyzed.

Animals

C57/BL6 mice were purchased from the Shanghai SLAC Laboratory animal company. *ChAT-IRES-Cre*, *Trpm5*-knockout / lac Z knockin (i.e., *Trpm5*$^{-/-}$), and *Ai9* (Jax stock numbers 006410, 005848 and 7909) were obtained from the Jackson laboratory. The *Gng13*$^{flox/flox}$ mice were generated previously (***Li et al. 2013***) and bred with the *ChAT-IRES-Cre* mice to conditionally knock out the *Gng13* gene in the choline acetyl-transferase (ChAT)-expressing cells of the *Gng13*-cKO mutant mice. Mice were bred to more than 98% of C57/BL6 genetic background and maintained under a 12-hour light/dark cycle with access to water and food ad libitum in the Laboratory Animal Center of Zhejiang University. Progeny was genotyped by PCR, and both male and female mice at 6 to 8 weeks old were used in the experiments. Studies involving animals were approved by the Zhejiang University Institutional Animal Care and Use Committee, and performed following the NIH "Guidelines for the Care and Use of Laboratory Animals".

Animal models of virally or chemically induced lung injury

Mice were anesthetized with 5% chloral hydrate (Sangon Biotech, A600288), and then intranasally administrated with 120 pfu of influenza virus A/Puerto Rico/8/1934 in 25 µl PBS at 0 day post infection (dpi). Control mice were intranasally instilled with 25 µl PBS only. The mice were checked every day and weighted every two days and euthanized for analysis at specific time points.

For chemically injured mouse models, mice were intraperitoneally administrated with a single dose of bleomycin (Selleck, s1214) at 6 mg/kg bodyweight, or first anesthetized and then injected into trachea with the house dust mite extract (Biolead, XPb70D3A2.5) at 2 mg/kg bodyweight, one dose per day for three consecutive days, or injected through trachea a single dose of lipopolysaccharide (LPS) (Sigma, L2630) at 1 mg/kg bodyweight. The lung tissues were dissected out for studies 14 days after the first injection.

Fluorescence-activated cell sorting

The heterogeneous *ChAT-Cre*: Ai9 mice at 25 dpi were anesthetized and transcardially perfused with cold PBS; their lungs were then isolated and dissociated into single cells as described previously (***Zhao et al. 2020***; ***Barkauskas et al. 2013***) . Briefly, the lung tissues were minced into pieces of 1 mm^3 by a pair of ophthalmic scissors, which were then digested with 1 mg/mL dispase II (Sigma, D4693), 3 mg/mL collagenase I (Sigma, C0130) and 0.5 mg/mL DNase I (Sigma, DN25) in DMEM/F12 medium (Thermo Fisher Scientific, C11330500BT) with 1% P/S for 50 min at 37 °C on a shaker. The cell suspension was then filtered by a 70-µm cell strainer (Biosharp, BS-70-XBS) and treated by red blood cell lysis buffer (Beyotime, C3702) for 3 min at room temperature. The cell suspension was then again filtered by a 40-µm cell strainer (Biosharp, BS-40-XBS), and the cells were collected and resuspended in the collection buffer (DPBS plus 0.04% BSA) (***Figure 2—figure Supplement 1***). Cell sorting and data analysis were performed on a Beckman Coulter FACS flow cytometer.

Immunohistochemistry

Lungs were harvested and processed as described previously (***Zhao et al. 2020***). Briefly, freshly dissected mouse lungs were fixed with 4% paraformaldehyde (PFA) at RT for 2.5 h on a shaker, followed by cryoprotection in 30% sucrose in PBS at 4 °C overnight. The lungs were incubated in 30% sucrose in PBS pre-mixed with an equal volume of optimal cutting temperature compound (OCT, Tissue-Tek) at RT for 2h on a shaker, and then embedded in 100% OCT and placed in a -80 °C freezer for 2 h, which were then sliced into 12μm-thick sections on a cryostat (Thermo scientific, HM525). The tissue sections were blocked in the blocking buffer (PBS plus 3% BSA, 0.3% Triton X-100, 2% donkey serum and 0.1% sodium azide) for 1h at RT, followed by incubation at 4°C overnight with primary antibodies diluted in the blocking buffer (rabbit anti-Dclk1 1:1000, Abcam, ab31704; rabbit anti-Dclk1-488 1:1000, Abcam, ab202754; rabbit anti-Gnat3 1:500, Santa Cruz Biotechnology, sc-395; rabbit anti-Plcβ2 1:500, Santa Cruz Biotechnology, sc-206; rabbit anti-CD45 1:500, Abcam, ab10558; rabbit anti-CD64 1:200, Thermo Fisher Scientific, MA5-29706; rabbit anti-Gsdmd 1:400, Affinity, AF4012; rabbit anti-Gsdme 1:500, Proteintech, 13075-1-AP; rabbit anti-F4/80-FITC 1:500, Thermo Fisher Scientific, 11-4801-81; rabbit anti-EpCAM 1:500, Thermo Fisher Scientific, 11-5791-82; rabbit anti-krt5 1:500, BioLegend, 905504). The slides were washed and incubated with the secondary antibodies: donkey anti-rabbit IgG H&L (Alexa Fluor® 488) 1:500, Abcam, ab150073; donkey anti-rabbit IgG H&L (Alexa Fluor® 568) 1:500, Abcam, ab175470, for 1.5h at RT. Fluorescent images were captured using an FV3000 laser scanning confocal microscope (Olympus) and VS200 slide scanner (Olympus).

Calcium imaging

TdTomato$^+$ cells were isolated and FACS-sorted as described above from the H1N1-infected *ChAT-Cre*: Ai9 mice. These cells were seeded on laminin-coated chambers and cultured in the imaging buffer (1X HBSS, 10 mM HEPES, 1mM sodium pyruvate) for 30 min. Cells were loaded with 5 μM fluorescent Ca^{2+}indicator Fluo-4 AM (Dojindo, F312) and Pluronic F-127 for 40 min at 37 °C, 5% CO_2, following the previously reported protocol (***Luo et al. 2019***). The cells were gently washed twice with HBSS to remove any excess Fluo-4 AM and Pluronic F-127. Denatonium benzoate (D.B. Sigma, D5765) and quinine (MedChemExpress, HY-D0143) were used as bitter substances. Allyl isothiocyanate (AITC Sigma, 36682), gallein (APExBIO, B7271) and U73122 (Sigma, U6756) were used as inhibitors for bitter taste receptor, G protein β subunit and Plcβ2 activity, respectively. The cells were first stimulated by the bitter compounds of 1 mM D.B. or 100 μM quinine, then blocked by incubating with 3 mM AITC, 100 μM gallein or 10 μM U73122 for 10 min before the inhibitors were removed; and D.B. or quinine applied again to assess the cells' calcium responsiveness. Images were captured with an excitation wavelength of 494 nm and emission wavelength of 516 nm using an IX83 total internal reflection fluorescence microscope (Olympus).

Bronchoalveolar lavage fluid (BALF) assays

BALF were prepared as previously described (***Akbari et al. 2003***). Briefly, after the trachea was exposed, 0.5 mL ice-cold PBS was gently instilled into the lung and then all the fluid was collected, which was repeated 3 times. A total of 1.5 mL BALF was collected, which was centrifuged at 300x g for 10 min at 4 °C. The supernatants were used to determine lactate dehydrogenase activity and IL-1β level using LDH-Glo^{TM} Cytotoxicity Assay (Promega, J2380) and Mouse IL-1 beta DuoSet ELISA (R&D Systems, DY401) following the manufacturer's instruction. The cells in the pellet were resuspended, a portion of which was used to count cells whereas the rest was used to extract proteins using RIPA buffer (Sangon Biotech, C500005); and the protein concentrations were determined by a BCA protein assay kit (Sangon Biotech, C503021) following the manufacturer's instruction.

Lung wet/dry weight (W/D) ratio

Mice were sacrificed with a lethal dose of 5% chloral hydrate. The lungs were isolated and cleaned to remove any adherent blood. The wet weight of lungs was immediately determined, followed by

drying in a heated stove at 65 °C for 48 h. The W/D ratio was calculated by dividing the wet lung weight by its corresponding dry weight.

Quantitative reverse transcription-PCR

Lungs from H1N1-infected and -uninfected mice were dissected out and washed 3 times with ice-cold PBS. The damaged lung areas of the infected mice and the corresponding lung areas of the uninfected control mice were excised to isolate total RNAs using TaKaRa MiniBEST Universal RNA Extraction Kit (TaKaRa, 9767), which were reverse transcribed into cDNAs using the RevertAid First Strand cDNA Synthesis Kit (Thermo Fisher Scientific, K1622). qPCR reactions were set up using iQ^{TM} SYBR Green Supermix (Bio-rad, 1708884), and run on the CFX Connect^{TM} Real-Time System. Relative expressions were calculated and normalized to the expression of an internal control gene *Actb*. The primer pairs used in these qPCR reactions are listed in ***Table 1***.

Western blotting

Lung lobes from H1N1-infected and -uninfected control mice were harvested. The damaged lung tissues from the infected mice and the tissues from the corresponding areas of the control lungs were collected to extract proteins using RIPA buffer (Sangon Biotech, C500005), which were centrifuged at 14,000×g for 25 min to remove any debris. The protein concentrations in the supernatants were determined using a BCA protein assay kit (Sangon Biotech, C503021), and an equal amount of protein, i.e., 20 or 40 μg from each sample was loaded onto a 10-12% SDS-PAGE gel for protein separation. The proteins on the gel were then transferred to PVDF membranes (Millipore, IPVH00010), which were blocked in 5% BSA for 1h at RT. The membranes then were incubated at 4°C overnight with the primary antibodies diluted in the blocking buffer (rabbit anti-NLRP3 1:1000, Abcam, ab263899; rabbit anti-Gsdmd 1:1000, Abcam, ab219800; mouse anti-caspase-1 1:1000, Santa Cruz Biotechnology, sc-56036; goat anti-IL-1β 1:800, R&D Systems, AF-401-SP; mouse anti-β-actin 1:1000, Beyotime, AA128-1), followed by incubation with the HRP-conjugated secondary antibodies (goat anti-rabbit 1:2000, Beyotime, A0208; donkey anti-goat 1:2000, Beyotime, A0181; goat anti-mouse 1:2000, Beyotime, A0216) for 1.5 h at RT. Protein bands on the membranes were visualized using a chemiluminescent imaging system (Tanon, 5200) and quantified using the ImageJ software.

Collagen deposition assay

Lung tissue sections were analyzed with hematoxylin and eosin (H&E) staining and Masson's trichrome staining for the assessment of the proportion of collagen content (***Jia et al. 2019***). Modified Masson's Trichrome Stain Kit (absin, abs9348) was used according to the manufacturer's instructions. The sections then were photographed using a multizoom AZ100 microscope (Nikon) and the Masson's trichrome-stained collagen areas were determined using the ImageJ software, divided by the total area of the section. For each treatment, 3 or more mice were used.

Sytox green staining

Each mouse was intranasally administrated with 1 mL 1× Sytox Green (Beyotime, C1070S) (***Halverson et al. 2015***). Ten minutes later, the lungs were harvested and cut into 12 μm-thick sections as previously described (***Zhao et al.***, 2020). Green fluorescence (Ex. 490; Em. 535) was measured using FV3000 laser scanning confocal microscope (Olympus).

Statistical analysis

Experimental data were obtained from three or more biological replicates, presented as mean ± SD using Graph Prism 9 software. Unpaired two-tailed Student's *t*-tests were performed and *P* values <0.05 were considered statistically significant. Animal survival rates were determined using the Kaplan-Meier method and data were analyzed with the log-rank test.

Acknowledgements

We thank All Huang Lab members for their helpful discussion and support.

Additional imformations

Funding

This research was in-part supported by
Starry Night Science Fund of Zhejiang University Shanghai Institute for Advanced Study Grant SN-ZJU-SIAS-005 (to LHuang) and SN-ZJU-SIAS-003 (to RZ)
National Key Research and Development Program of China Grant 2021YFF1200803 (to LHuang), 2021YFF1200404 and 2021YFA1201200 (to RZ)
National Natural Science Foundation of China U1967217 (to RZ)
National Center of Technology Innovation for Biopharmaceuticals NCTIB2022HS02010 (to RZ)
National Independent Innovation Demonstration Zone Shanghai Zhangjiang Major Projects ZJZX2020014 (to RZ)

Author contributions

Conceptualization: LHuang, RZ, YHL
Methodology: LHuang, YHL, YSY, YBX, HLei, YY, SSZ
Investigation: YHL, YSY, YBX, HLei, SSZ, JQ
Visualization: YHL, YSY, YBX, JQ
Supervision: LHuang, RZ
Writing—original draft: YHL, YSY, LHuang, RZ
Writing—review & editing: LHuang, RZ

Competing interests

The authors declare that they have no competing interests.

Data and materials availability

All data needed to evaluate the conclusions in the paper are present in the paper and/or the Supplementary Materials. Additional data related to this paper may be requested from the authors.

Additional files

This PDF file includes: ***Figure 1—figure Supplement 1*** to ***Figure 5—figure Supplement 2***, ***Table 1***

References

Adler E, Hoon MA, Mueller KL, Chandrashekar J, Ryba NJ, Zuker CS. A novel family of mammalian taste receptors. Cell. 2000; 100(6):693–702. https://www.ncbi.nlm.nih.gov/pubmed/10761934, doi: http://dx.doi.org/10.1016/s0092-8674(00)80705-9.

Akbari O, Stock P, Meyer E, Kronenberg M, Sidobre S, Nakayama T, Taniguchi M, Grusby MJ, DeKruyff RH, Umetsu DT. Essential role of NKT cells producing IL-4 and IL-13 in the development of allergen-induced airway hyperreactivity. Nat Med. 2003; 9(5):582–8. https://www.nature.com/articles/nm851, doi: http://dx.doi.org/10.1038/nm851.

Banerjee A, McKinley ET, von Moltke J, Coffey RJ, Lau KS. Interpreting heterogeneity in intestinal tuft cell structure and function. J Clin Invest. 2018; 128(5):1711–1719. https://www.ncbi.nlm.nih.gov/pubmed/29714721, doi: http://dx.doi.org/10.1172/JCI120330.

Bankova LG, Boyce JA. A new spin on mast cells and cysteinyl leukotrienes: Leukotriene E(4) activates mast cells in vivo. J Allergy Clin Immunol. 2018; 142(4):1056–1057. https://www.ncbi.nlm.nih.gov/pubmed/30165055, doi: http://dx.doi.org/10.1016/j.jaci.2018.08.008.

Bankova LG, Dwyer DF, Yoshimoto E, Ualiyeva S, McGinty JW, Raff H, von Moltke J, Kanaoka Y, Frank Austen K, Barrett NA. The cysteinyl leukotriene 3 receptor regulates expansion of IL-25-producing airway brush cells leading to type 2 inflammation. Sci Immunol. 2018; 3(28):eaat9453. https://www.ncbi.nlm.nih.gov/pubmed/30291131, doi: http://dx.doi.org/10.1126/sciimmunol.aat9453.

Barkauskas CE, Cronce MJ, Rackley CR, Bowie EJ, Keene DR, Stripp BR, Randell SH, Noble PW, Hogan BL. Type 2 alveolar cells are stem cells in adult lung. J Clin Invest. 2013; 123(7):3025–36. https://www.ncbi.nlm.nih.gov/pubmed/23921127, doi: http://dx.doi.org/10.1172/JCI68782.

Barr J, Gentile ME, Lee S, Kotas ME, Fernanda de Mello Costa M, Holcomb NP, Jaquish A, Palashikar G, Soewignjo M, McDaniel M, Matsumoto I, Margolskee R, Von Moltke J, Cohen NA, Sun X, Vaughan AE. Injury-induced pulmonary tuft cells are heterogenous, arise independent of key Type 2 cytokines, and are dispensable for dysplastic repair. Elife. 2022; 11:e78074. https://www.ncbi.nlm.nih.gov/pubmed/36073526, doi: http://dx.doi.org/10.7554/eLife.78074.

Bezencon C, Furholz A, Raymond F, Mansourian R, Metairon S, Le Coutre J, Damak S. Murine intestinal cells expressing Trpm5 are mostly brush cells and express markers of neuronal and inflammatory cells. J Comp Neurol. 2008; 509(5):514–25. http://www.ncbi.nlm.nih.gov/pubmed/18537122, doi: http://dx.doi.org/10.1002/cne.21768.

Billipp TE, Nadjsombati MS, von Moltke J. Tuning tuft cells: new ligands and effector functions reveal tissue-specific function. Curr Opin Immunol. 2021; 68:98–106. https://www.ncbi.nlm.nih.gov/pubmed/33166855, doi: http://dx.doi.org/10.1016/j.coi.2020.09.006.

Campbell AP, Smrcka AV. Targeting G protein-coupled receptor signalling by blocking G proteins. Nat Rev Drug Discov. 2018; 17(11):789–803. https://www.ncbi.nlm.nih.gov/pubmed/30262890, doi: http://dx.doi.org/10.1038/nrd.2018.135.

Carey RM, Lee RJ. Taste Receptors in Upper Airway Innate Immunity. Nutrients. 2019; 11(9):2017. https://www.ncbi.nlm.nih.gov/pubmed/31466230, doi: http://dx.doi.org/10.3390/nu11092017.

Chandrashekar J, Mueller KL, Hoon MA, Adler E, Feng L, Guo W, Zuker CS, Ryba NJ. T2Rs function as bitter taste receptors. Cell. 2000; 100(6):703–11. https://www.ncbi.nlm.nih.gov/pubmed/10761935, doi: http://dx.doi.org/10.1016/s0092-8674(00)80706-0.

Chen G, Wu D, Guo W, Cao Y, Huang D, Wang H, Wang T, Zhang X, Chen H, Yu H, Zhang X, Zhang M, Wu S, Song J, Chen T, Han M, Li S, Luo X, Zhao J, Ning Q. Clinical and immunological features of severe and moderate coronavirus disease 2019. J Clin Invest. 2020; 130(5):2620–2629. https://www.ncbi.nlm.nih.gov/pubmed/32217835, doi: http://dx.doi.org/10.1172/JCI137244.

Codagnone M, Cianci E, Lamolinara A, Mari VC, Nespoli A, Isopi E, Mattoscio D, Arita M, Bragonzi A, Iezzi M, Romano M, Recchiuti A. Resolvin D1 enhances the resolution of lung inflammation caused by long-term Pseudomonas aeruginosa infection. Mucosal Immunol. 2018; 11(1):35–49. https://www.ncbi.nlm.nih.gov/pubmed/28422188, doi: http://dx.doi.org/10.1038/mi.2017.36.

Damak S, Rong M, Yasumatsu K, Kokrashvili Z, Perez CA, Shigemura N, Yoshida R, Mosinger J B, Glendinning JI, Ninomiya Y, Margolskee RF. Trpm5 null mice respond to bitter, sweet, and umami compounds. Chem Senses. 2006; 31(3):253–64. https://www.ncbi.nlm.nih.gov/pubmed/16436689, doi: http://dx.doi.org/10.1093/chemse/bjj027.

DelGiorno KE, Naeem RF, Fang L, Chung CY, Ramos C, Luhtala N, O'Connor C, Hunter T, Manor U, Wahl GM. Tuft Cell Formation Reflects Epithelial Plasticity in Pancreatic Injury: Implications for Modeling Human Pancreatitis. Front Physiol. 2020; 11:88. https://www.ncbi.nlm.nih.gov/pubmed/32116793, doi: http://dx.doi.org/10.3389/fphys.2020.00088.

Donaldson LJ, Rutter PD, Ellis BM, Greaves FE, Mytton OT, Pebody RG, Yardley IE. Mortality from pandemic A/H1N1 2009 influenza in England: public health surveillance study. BMJ. 2009; 339:b5213. https://www.ncbi.nlm.nih.gov/pubmed/20007665, doi: http://dx.doi.org/10.1136/bmj.b5213.

Doyle ME, Premathilake HU, Yao Q, Mazucanti CH, Egan JM. Physiology of the tongue with emphasis on taste transduction. Physiol Rev. 2023; 103(2):1193–1246. https://www.ncbi.nlm.nih.gov/pubmed/36422992, doi: http://dx.doi.org/10.1152/physrev.00012.2022.

Finger TE, Bottger B, Hansen A, Anderson KT, Alimohammadi H, Silver WL. Solitary chemoreceptor cells in the nasal cavity serve as sentinels of respiration. Proc Natl Acad Sci U S A. 2003; 100(15):8981–6. https://www.ncbi.nlm.nih.gov/pubmed/12857948, doi: http://dx.doi.org/10.1073/pnas.1531172100.

Finger TE, Danilova V, Barrows J, Bartel DL, Vigers AJ, Stone L, Hellekant G, Kinnamon SC. ATP signaling is crucial for communication from taste buds to gustatory nerves. Science. 2005; 310(5753):1495–9. https://www.ncbi.nlm.nih.gov/pubmed/16322458, doi: http://dx.doi.org/10.1126/science.1118435.

Gerbe F, Sidot E, Smyth DJ, Ohmoto M, Matsumoto I, Dardalhon V, Cesses P, Garnier L, Pouzolles M, Brulin B, Bruschi M, Harcus Y, Zimmermann VS, Taylor N, Maizels RM, Jay P. Intestinal epithelial tuft cells initiate type 2 mucosal immunity to helminth parasites. Nature. 2016; 529(7585):226–30. http://www.ncbi.nlm.nih.gov/pubmed/26762460, doi: http://dx.doi.org/10.1038/nature16527.

Haber AL, Biton M, Rogel N, Herbst RH, Shekhar K, Smillie C, Burgin G, Delorey TM, Howitt MR, Katz Y, Tirosh I, Beyaz S, Dionne D, Zhang M, Raychowdhury R, Garrett WS, Rozenblatt-Rosen O, Shi HN, Yilmaz O, Xavier RJ, et al. A single-cell survey of the small intestinal epithelium. Nature. 2017; 551(7680):333–339. http://www.ncbi.nlm.nih.gov/pubmed/29144463, doi: http://dx.doi.org/10.1038/nature24489.

Halverson TW, Wilton M, Poon KK, Petri B, Lewenza S. DNA is an antimicrobial component of neutrophil extracellular traps. PLoS Pathog. 2015; 11(1):e1004593. https://www.ncbi.nlm.nih.gov/pubmed/25590621, doi: http://dx.doi.org/10.1371/journal.ppat.1004593.

Hollenhorst MI, Jurastow I, Nandigama R, Appenzeller S, Li L, Vogel J, Wiederhold S, Althaus M, Empting M, Altmuller J, Hirsch AKH, Flockerzi V, Canning BJ, Saliba AE, Krasteva-Christ G. Tracheal brush cells release acetylcholine in response to bitter tastants for paracrine and autocrine signaling. FASEB J. 2020; 34(1):316–332. https://www.ncbi.nlm.nih.gov/pubmed/31914675, doi: http://dx.doi.org/10.1096/fj.201901314RR.

Hollenhorst MI, Krasteva-Christ G. Chemosensory cells in the respiratory tract as crucial regulators of innate immune responses. J Physiol. 2023; 601(9):1555–1572. https://www.ncbi.nlm.nih.gov/pubmed/37009787, doi: http://dx.doi.org/10.1113/JP282307.

Hollenhorst MI, Nandigama R, Evers SB, Gamayun I, Abdel Wadood N, Salah A, Pieper M, Wyatt A, Stukalov A, Gebhardt A, Nadolni W, Burow W, Herr C, Beisswenger C, Kusumakshi S, Ectors F, Kichko TI, Hubner L, Reeh P, Munder A, et al. Bitter taste signaling in tracheal epithelial brush cells elicits innate immune responses to bacterial infection. J Clin Invest. 2022; 132(13):e150951. https://www.ncbi.nlm.nih.gov/pubmed/35503420, doi: http://dx.doi.org/10.1172/JCI150951.

Howitt MR, Cao YG, Gologorsky MB, Li JA, Haber AL, Biton M, Lang J, Michaud M, Regev A, Garrett WS. The Taste Receptor TAS1R3 Regulates Small Intestinal Tuft Cell Homeostasis. Immunohorizons. 2020; 4(1):23–32. https://www.ncbi.nlm.nih.gov/pubmed/31980480, doi: http://dx.doi.org/10.4049/immunohorizons.1900099.

Howitt MR, Lavoie S, Michaud M, Blum AM, Tran SV, Weinstock JV, Gallini CA, Redding K, Margolskee RF, Osborne LC, Artis D, Garrett WS. Tuft cells, taste-chemosensory cells, orchestrate parasite type 2 immunity in the gut. Science. 2016; 351(6279):1329–33. https://www.ncbi.nlm.nih.gov/pubmed/26847546, doi: http://dx.doi.org/10.1126/science.aaf1648.

Huang H, Fang Y, Jiang M, Zhang Y, Biermann J, Melms JC, Danielsson JA, Yang Y, Qiang L, Liu J, Zhou Y, Wang M, Hu Z, Wang TC, Saqi A, Sun J, Matsumoto I, Cardoso WV, Emala CW, Zhu J, et al. Contribution of Trp63(CreERT2)-labeled cells to alveolar regeneration is independent of tuft cells. Elife. 2022; 11:e78217. https://www.ncbi.nlm.nih.gov/pubmed/36129169, doi: http://dx.doi.org/10.7554/eLife.78217.

Huang L, Shanker YG, Dubauskaite J, Zheng JZ, Yan W, Rosenzweig S, Spielman AI, Max M, Margolskee RF. Ggamma13 colocalizes with gustducin in taste receptor cells and mediates IP3 responses to bitter denatonium. Nat Neurosci. 1999; 2(12):1055–62. https://pubmed.ncbi.nlm.nih.gov/10570481/, doi: http://dx.doi.org/10.1038/15981.

Imai H, Hakukawa M, Hayashi M, Iwatsuki K, Masuda K. Expression of Bitter Taste Receptors in the Intestinal Cells of Non-Human Primates. Int J Mol Sci. 2020; 21(3):902. https://www.ncbi.nlm.nih.gov/pubmed/32019181, doi: http://dx.doi.org/10.3390/ijms21030902.

Jia Q, Cao H, Shen D, Li S, Yan L, Chen C, Xing S, Dou F. Quercetin protects against atherosclerosis by regulating the expression of PCSK9, CD36, PPARgamma, LXRalpha and ABCA1. Int J Mol Med. 2019; 44(3):893–902. https://www.ncbi.nlm.nih.gov/pubmed/31524223, doi: http://dx.doi.org/10.3892/ijmm.2019.4263.

Kankanamge D, Tennakoon M, Karunarathne A, Gautam N. G protein gamma subunit, a hidden master regulator of GPCR signaling. J Biol Chem. 2022; 298(12):102618. https://www.ncbi.nlm.nih.gov/pubmed/36272647, doi: http://dx.doi.org/10.1016/j.jbc.2022.102618.

Keshavarz M, Faraj Tabrizi S, Ruppert AL, Pfeil U, Schreiber Y, Klein J, Brandenburger I, Lochnit G, Bhushan S, Perniss A, Deckmann K, Hartmann P, Meiners M, Mermer P, Rafiq A, Winterberg S, Papadakis T, Thomas D, Angioni C, Oberwinkler J, et al. Cysteinyl leukotrienes and acetylcholine are biliary tuft cell co-transmitters. Sci Immunol. 2022; 7(69):eabf6734. https://www.ncbi.nlm.nih.gov/pubmed/35245090, doi: http://dx.doi.org/10.1126/sciimmunol.abf6734.

Kotas ME, Moore CM, Gurrola n J G, Pletcher SD, Goldberg AN, Alvarez R, Yamato S, Bratcher PE, Shaughnessy CA, Zeitlin PL, Zhang IH, Li Y, Montgomery MT, Lee K, Cope EK, Locksley RM, Seibold MA, Gordon ED. IL-13-programmed airway tuft cells produce PGE2, which promotes CFTR-dependent mucociliary function. JCI Insight. 2022; 7(13):e159832. https://www.ncbi.nlm.nih.gov/pubmed/35608904, doi: http://dx.doi.org/10.1172/jci.insight.159832.

Krasteva G, Canning BJ, Hartmann P, Veres TZ, Papadakis T, Muhlfeld C, Schliecker K, Tallini YN, Braun A, Hackstein H, Baal N, Weihe E, Schutz B, Kotlikoff M, Ibanez-Tallon I, Kummer W. Cholinergic chemosensory cells in the trachea regulate breathing. Proc Natl Acad Sci U S A. 2011; 108(23):9478–83. https://www.ncbi.nlm.nih.gov/pubmed/21606356, doi: http://dx.doi.org/10.1073/pnas.1019418108.

Krishnamoorthy N, Walker KH, Bruggemann TR, Tavares LP, Smith EW, Nijmeh J, Bai Y, Ai X, Cagnina RE, Duvall MG, Lehoczky JA, Levy BD. The Maresin 1-LGR6 axis decreases respiratory syncytial virus-induced lung inflammation. Proc Natl Acad Sci U S A. 2023; 120(2):e2206480120. https://www.ncbi.nlm.nih.gov/pubmed/36595677, doi: http://dx.doi.org/10.1073/pnas.2206480120.

Lee RJ, Kofonow JM, Rosen PL, Siebert AP, Chen B, Doghramji L, Xiong G, Adappa ND, Palmer JN, Kennedy DW, Kreindler JL, Margolskee RF, Cohen NA. Bitter and sweet taste receptors regulate human upper respiratory innate immunity. J Clin Invest. 2014; 124(3):1393–405. https://www.ncbi.nlm.nih.gov/pubmed/24531552, doi: http://dx.doi.org/10.1172/JCI72094.

Lei W, Ren W, Ohmoto M, Urban J J F, Matsumoto I, Margolskee RF, Jiang P. Activation of intestinal tuft cell-expressed Sucnr1 triggers type 2 immunity in the mouse small intestine. Proc Natl Acad Sci U S A. 2018; 115(21):5552–5557. http://www.ncbi.nlm.nih.gov/pubmed/29735652, doi: http://dx.doi.org/10.1073/pnas.1720758115.

Li F, Ponissery-Saidu S, Yee KK, Wang H, Chen ML, Iguchi N, Zhang G, Jiang P, Reisert J, Huang L. Heterotrimeric G protein subunit Ggamma13 is critical to olfaction. J Neurosci. 2013; 33(18):7975–84. https://www.ncbi.nlm.nih.gov/pubmed/23637188, doi: http://dx.doi.org/10.1523/JNEUROSCI.5563-12.2013.

Liman ER. Trpm5. Handb Exp Pharmacol. 2014; 222:489–502. https://www.ncbi.nlm.nih.gov/pubmed/24756718, doi: http://dx.doi.org/10.1007/978-3-642-54215-2_19.

Lindemann B. Taste reception. Physiol Rev. 1996; 76(3):719–66. https://www.ncbi.nlm.nih.gov/pubmed/8757787, doi: http://dx.doi.org/10.1152/physrev.1996.76.3.719.

Lossow K, Hubner S, Roudnitzky N, Slack JP, Pollastro F, Behrens M, Meyerhof W. Comprehensive Analysis of Mouse Bitter Taste Receptors Reveals Different Molecular Receptive Ranges for Orthologous Receptors in Mice and Humans. J Biol Chem. 2016; 291(29):15358–77. https://www.ncbi.nlm.nih.gov/pubmed/27226572, doi: http://dx.doi.org/10.1074/jbc.M116.718544.

Luo XC, Chen ZH, Xue JB, Zhao DX, Lu C, Li YH, Li SM, Du YW, Liu Q, Wang P, Liu M, Huang L. Infection by the parasitic helminth Trichinella spiralis activates a Tas2r-mediated signaling pathway in intestinal tuft cells. Proc Natl Acad Sci U S A. 2019; 116(12):5564–5569. https://www.ncbi.nlm.nih.gov/pubmed/30819885, doi: http://dx.doi.org/10.1073/pnas.1812901116.

Matsumoto I, Ohmoto M, Narukawa M, Yoshihara Y, Abe K. Skn-1a (Pou2f3) specifies taste receptor cell lineage. Nat Neurosci. 2011; 14(6):685–7. https://www.ncbi.nlm.nih.gov/pubmed/21572433, doi: http://dx.doi.org/10.1038/nn.2820.

Matsunami H, Montmayeur JP, Buck LB. A family of candidate taste receptors in human and mouse. Nature. 2000; 404(6778):601–4. https://www.ncbi.nlm.nih.gov/pubmed/10766242, doi: http://dx.doi.org/10.1038/35007072.

Max M, Shanker YG, Huang L, Rong M, Liu Z, Campagne F, Weinstein H, Damak S, Margolskee RF. Tas1r3, encoding a new candidate taste receptor, is allelic to the sweet responsiveness locus Sac. Nat Genet. 2001; 28(1):58–63. https://www.ncbi.nlm.nih.gov/pubmed/11326277, doi: http://dx.doi.org/10.1038/ng0501-58.

McGinty JW, Ting HA, Billipp TE, Nadjsombati MS, Khan DM, Barrett NA, Liang HE, Matsumoto I, von Moltke J. Tuft-Cell-Derived Leukotrienes Drive Rapid Anti-helminth Immunity in the Small Intestine but Are Dispensable for Anti-protist Immunity. Immunity. 2020; 52(3):528–541 e7. https://www.ncbi.nlm.nih.gov/pubmed/32160525, doi: http://dx.doi.org/10.1016/j.immuni.2020.02.005.

Melms JC, Biermann J, Huang H, Wang Y, Nair A, Tagore S, Katsyv I, Rendeiro AF, Amin AD, Schapiro D, Frangieh CJ, Luoma AM, Filliol A, Fang Y, Ravichandran H, Clausi MG, Alba GA, Rogava M, Chen SW, Ho P, et al. A molecular single-cell lung atlas of lethal COVID-19. Nature. 2021; 595(7865):114–119. https://www.ncbi.nlm.nih.gov/pubmed/33915568, doi: http://dx.doi.org/10.1038/s41586-021-03569-1.

Miller CN, Proekt I, von Moltke J, Wells KL, Rajpurkar AR, Wang H, Rattay K, Khan IS, Metzger TC, Pollack JL, Fries AC, Lwin WW, Wigton EJ, Parent AV, Kyewski B, Erle DJ, Hogquist KA, Steinmetz LM, Locksley RM, Anderson MS. Thymic tuft cells promote an IL-4-enriched medulla and shape thymocyte development. Nature. 2018; 559(7715):627–631. https://www.ncbi.nlm.nih.gov/pubmed/30022164, doi: http://dx.doi.org/10.1038/s41586-018-0345-2.

von Moltke J, Ji M, Liang HE, Locksley RM. Tuft-cell-derived IL-25 regulates an intestinal ILC2-epithelial response circuit. Nature. 2016; 529(7585):221–5. https://www.ncbi.nlm.nih.gov/pubmed/26675736, doi: http://dx.doi.org/10.1038/nature16161.

Montoro DT, Haber AL, Biton M, Vinarsky V, Lin B, Birket SE, Yuan F, Chen S, Leung HM, Villoria J, Rogel N, Burgin G, Tsankov AM, Waghray A, Slyper M, Waldman J, Nguyen L, Dionne D, Rozenblatt-Rosen O, Tata PR, et al. A revised airway epithelial hierarchy includes CFTR-expressing ionocytes. Nature. 2018; 560(7718):319–324. https://www.ncbi.nlm.nih.gov/pubmed/30069044, doi: http://dx.doi.org/10.1038/s41586-018-0393-7.

Nadjsombati MS, McGinty JW, Lyons-Cohen MR, Jaffe JB, DiPeso L, Schneider C, Miller CN, Pollack JL, Nagana Gowda GA, Fontana MF, Erle DJ, Anderson MS, Locksley RM, Raftery D, von Moltke J. Detection of Succinate by Intestinal Tuft Cells Triggers a Type 2 Innate Immune Circuit. Immunity. 2018; 49(1):33–41 e7. https://www.ncbi.nlm.nih.gov/pubmed/30021144, doi: http://dx.doi.org/10.1016/j.immuni.2018.06.016.

Nakano H, Hata A, Ishimura U, Kosugi R, Miyamoto E, Nakamura K, Muramatsu T, Ogasawara M, Yamada M, Umemura M, Takahashi S, Takahashi Y. Activating transcription factor 5 (ATF5) controls intestinal tuft and goblet cell expansion upon succinate-induced type 2 immune responses in mice. Cell Tissue Res. 2023; 393(2):343–355. https://www.ncbi.nlm.nih.gov/pubmed/37256362, doi: http://dx.doi.org/10.1007/s00441-023-03781-7.

Nevalainen TJ. Ultrastructural characteristics of tuft cells in mouse gallbladder epithelium. Acta Anat (Basel). 1977; 98(2):210–20. https://www.ncbi.nlm.nih.gov/pubmed/871082, doi: http://dx.doi.org/10.1159/000144796.

O'Leary CE, Schneider C, Locksley RM. Tuft Cells-Systemically Dispersed Sensory Epithelia Integrating Immune and Neural Circuitry. Annu Rev Immunol. 2019; 37:47–72. https://www.ncbi.nlm.nih.gov/pubmed/30379593, doi: http://dx.doi.org/10.1146/annurev-immunol-042718-041505.

Panigrahy D, Gilligan MM, Serhan CN, Kashfi K. Resolution of inflammation: An organizing principle in biology and medicine. Pharmacol Ther. 2021; 227:107879. https://www.ncbi.nlm.nih.gov/pubmed/33915177, doi: http://dx.doi.org/10.1016/j.pharmthera.2021.107879.

Peiris JS. Severe Acute Respiratory Syndrome (SARS). J Clin Virol. 2003; 28(3):245–7. https://www.ncbi.nlm.nih.gov/pubmed/14522062, doi: http://dx.doi.org/10.1016/j.jcv.2003.08.005.

Perniss A, Boonen B, Tonack S, Thiel M, Poharkar K, Alnouri MW, Keshavarz M, Papadakis T, Wiegand S, Pfeil U, Richter K, Althaus M, Oberwinkler J, Schutz B, Boehm U, Offermanns S, Leinders-Zufall T, Zufall F, Kummer W. A succinate/SUCNR1-brush cell defense program in the tracheal epithelium. Sci Adv. 2023; 9(31):eadg8842. https://www.ncbi.nlm.nih.gov/pubmed/37531421, doi: http://dx.doi.org/10.1126/sciadv.adg8842.

Rane CK, Jackson SR, Pastore CF, Zhao G, Weiner AI, Patel NN, Herbert DR, Cohen NA, Vaughan AE. Development of solitary chemosensory cells in the distal lung after severe influenza injury. Am J Physiol Lung Cell Mol Physiol. 2019; 316(6):L1141–L1149. https://www.ncbi.nlm.nih.gov/pubmed/30908939, doi: http://dx.doi.org/10.1152/ajplung.00032.2019.

Roach SN, Fiege JK, Shepherd FK, Wiggen TD, Hunter RC, Langlois RA. Respiratory Influenza Virus Infection Causes Dynamic Tuft Cell and Innate Lymphoid Cell Changes in the Small Intestine. J Virol. 2022; 96(9):e0035222. https://www.ncbi.nlm.nih.gov/pubmed/35446142, doi: http://dx.doi.org/10.1128/jvi.00352-22.

Saqui-Salces M, Keeley TM, Grosse AS, Qiao XT, El-Zaatari M, Gumucio DL, Samuelson LC, Merchant JL. Gastric tuft cells express DCLK1 and are expanded in hyperplasia. Histochem Cell Biol. 2011; 136(2):191–204. https://www.ncbi.nlm.nih.gov/pubmed/21688022, doi: http://dx.doi.org/10.1007/s00418-011-0831-1.

Saunders CJ, Christensen M, Finger TE, Tizzano M. Cholinergic neurotransmission links solitary chemosensory cells to nasal inflammation. Proc Natl Acad Sci U S A. 2014; 111(16):6075–80. http://www.ncbi.nlm.nih.gov/pubmed/24711432, doi: http://dx.doi.org/10.1073/pnas.1402251111.

Schneider C, O'Leary CE, von Moltke J, Liang HE, Ang QY, Turnbaugh PJ, Radhakrishnan S, Pellizzon M, Ma A, Locksley RM. A Metabolite-Triggered Tuft Cell-ILC2 Circuit Drives Small Intestinal Remodeling. Cell. 2018; 174(2):271–284. https://www.ncbi.nlm.nih.gov/pubmed/29887373, doi: http://dx.doi.org/10.1016/j.cell.2018.05.014.

Serhan CN, Gupta SK, Perretti M, Godson C, Brennan E, Li Y, Soehnlein O, Shimizu T, Werz O, Chiurchiu V, Azzi A, Dubourdeau M, Gupta SS, Schopohl P, Hoch M, Gjorgevikj D, Khan FM, Brauer D, Tripathi A, Cesnulevicius K, et al. The Atlas of Inflammation Resolution (AIR). Mol Aspects Med. 2020; 74:100894. https://www.ncbi.nlm.nih.gov/pubmed/32893032, doi: http://dx.doi.org/10.1016/j.mam.2020.100894.

Serhan CN, de la Rosa X, Jouvene CC. Cutting Edge: Human Vagus Produces Specialized Proresolving Mediators of Inflammation with Electrical Stimulation Reducing Proinflammatory Eicosanoids. J Immunol. 2018; 201(11):3161–3165. https://www.ncbi.nlm.nih.gov/pubmed/30355784, doi: http://dx.doi.org/10.4049/jimmunol.1800806.

Tizzano M, Dvoryanchikov G, Barrows JK, Kim S, Chaudhari N, Finger TE. Expression of Galpha14 in sweet-transducing taste cells of the posterior tongue. BMC Neurosci. 2008; 9:110. https://www.ncbi.nlm.nih.gov/pubmed/19014514, doi: http://dx.doi.org/10.1186/1471-2202-9-110.

Tizzano M, Finger TE. Chemosensors in the nose: guardians of the airways. Physiology (Bethesda). 2013; 28(1):51–60. https://www.ncbi.nlm.nih.gov/pubmed/23280357, doi: http://dx.doi.org/10.1152/physiol.00035.2012.

Tizzano M, Gulbransen BD, Vandenbeuch A, Clapp TR, Herman JP, Sibhatu HM, Churchill ME, Silver WL, Kinnamon SC, Finger TE. Nasal chemosensory cells use bitter taste signaling to detect irritants and bacterial signals. Proc Natl Acad Sci U S A. 2010; 107(7):3210–5. https://www.ncbi.nlm.nih.gov/pubmed/20133764, doi: http://dx.doi.org/10.1073/pnas.0911934107.

Ualiyeva S, Hallen N, Kanaoka Y, Ledderose C, Matsumoto I, Junger WG, Barrett NA, Bankova LG. Airway brush cells generate cysteinyl leukotrienes through the ATP sensor P2Y2. Sci Immunol. 2020; 5(43):eaax7224. https://www.ncbi.nlm.nih.gov/pubmed/31953256, doi: http://dx.doi.org/10.1126/sciimmunol.aax7224.

Ualiyeva S, Lemire E, Aviles EC, Wong C, Boyd AA, Lai J, Liu T, Matsumoto I, Barrett NA, Boyce JA, Haber AL, Bankova LG. Tuft cell-produced cysteinyl leukotrienes and IL-25 synergistically initiate lung type 2 inflammation. Sci Immunol. 2021; 6(66):eabj0474. https://www.ncbi.nlm.nih.gov/pubmed/34932383, doi: http://dx.doi.org/10.1126/sciimmunol.abj0474.

Vaughan AE, Brumwell AN, Xi Y, Gotts JE, Brownfield DG, Treutlein B, Tan K, Tan V, Liu FC, Looney MR, Matthay MA, Rock JR, Chapman HA. Lineage-negative progenitors mobilize to regenerate lung epithelium after major injury. Nature. 2015; 517(7536):621–5. https://www.ncbi.nlm.nih.gov/pubmed/25533958, doi: http://dx.doi.org/10.1038/nature14112.

Wong GT, Gannon KS, Margolskee RF. Transduction of bitter and sweet taste by gustducin. Nature. 1996; 381(6585):796–800. https://www.ncbi.nlm.nih.gov/pubmed/8657284, doi: http://dx.doi.org/10.1038/381796a0.

Wu XS, He XY, Ipsaro JJ, Huang YH, Preall JB, Ng D, Shue YT, Sage J, Egeblad M, Joshua-Tor L, Vakoc CR. OCA-T1 and OCA-T2 are coactivators of POU2F3 in the tuft cell lineage. Nature. 2022; 607(7917):169–175. https://www.ncbi.nlm.nih.gov/pubmed/35576971, doi: http://dx.doi.org/10.1038/s41586-022-04842-7.

Xiong Z, Zhu X, Geng J, Xu Y, Wu R, Li C, Fan D, Qin X, Du Y, Tian Y, Fan Z. Intestinal Tuft-2 cells exert antimicrobial immunity via sensing bacterial metabolite N-undecanoylglycine. Immunity. 2022; 55(4):686–700 e7. https://www.ncbi.nlm.nih.gov/pubmed/35320705, doi: http://dx.doi.org/10.1016/j.immuni.2022.03.001.

Yamashita J, Ohmoto M, Yamaguchi T, Matsumoto I, Hirota J. Skn-1a/Pou2f3 functions as a master regulator to generate Trpm5-expressing chemosensory cells in mice. PLoS One. 2017; 12(12):e0189340. https://www.ncbi.nlm.nih.gov/pubmed/29216297, doi: http://dx.doi.org/10.1371/journal.pone.0189340.

Yunis J, Short KR, Yu D. Severe respiratory viral infections: T-cell functions diverging from immunity to inflammation. Trends Microbiol. 2023; 31(6):644–656. https://www.ncbi.nlm.nih.gov/pubmed/36635162, doi: http://dx.doi.org/10.1016/j.tim.2022.12.008.

Zhang Y, Hoon MA, Chandrashekar J, Mueller KL, Cook B, Wu D, Zuker CS, Ryba NJ. Coding of sweet, bitter, and umami tastes: different receptor cells sharing similar signaling pathways. Cell. 2003; 112(3):293–301. https://www.ncbi.nlm.nih.gov/pubmed/12581520, doi: http://dx.doi.org/10.1016/s0092-8674(03)00071-0.

Zhang Z, Zhao Z, Margolskee R, Liman E. The transduction channel TRPM5 is gated by intracellular calcium in taste cells. J Neurosci. 2007; 27(21):5777–86. https://www.ncbi.nlm.nih.gov/pubmed/17522321, doi: http://dx.doi.org/10.1523/JNEUROSCI.4973-06.2007.

Zhao G, Weiner AI, Neupauer KM, de Mello Costa MF, Palashikar G, Adams-Tzivelekidis S, Mangalmurti NS, Vaughan AE. Regeneration of the pulmonary vascular endothelium after viral pneumonia requires COUP-TF2. Sci Adv. 2020; 6(48):eabc4493. https://www.ncbi.nlm.nih.gov/pubmed/33239293, doi: http://dx.doi.org/10.1126/sciadv.abc4493.

Zhao GQ, Zhang Y, Hoon MA, Chandrashekar J, Erlenbach I, Ryba NJ, Zuker CS. The receptors for mammalian sweet and umami taste. Cell. 2003; 115(3):255–66. https://www.ncbi.nlm.nih.gov/pubmed/14636554, doi: http://dx.doi.org/10.1016/s0092-8674(03)00844-4.

Table 1. Sequences of primers used for qPCR

Species	Gene name	Sequences(5'-3')	Sequences(5'-3')
Mouse	Tas2r102	F:CTCCTGCTAATCTTCTCTTTGTG	R:GGGTCTCTGTGTCTTCTGG
	Tas2r103	F:AGCACAGTGGCCCACATAAA	R:TGGCCTGTGGGAAAAGCTAC
	Tas2r104	F:GCAACACATCCTGGCTGAT	R:CCCCATATTGGCAAAAACAT
	Tas2r105	F:CAGAAGGCATCCTCCTTTCCA	R:GCCCAGTCCATGCAGTTTAC
	Tas2r106	F:AGCCACATTCTTCTCAACCT	R:AGCATGTAATGATAGCCACCA
	Tas2r107	F:CTGGTTTGACAGCCACATGC	R:TGCCTTCAAAGAGGCTTGCT
	Tas2r108	F:GTTTCTCCTGTTGAAACGGACT	R:GTGAGGGCTGAAATCAGAAGA
	Tas2r109	F:GTCAAATTCAGGTGTTAGGAAGTC	R:CACAGGGAGAAGATGAGCAG
	Tas2r110	F:AGGTCAATGCCAAACCACCT	R:CAGCAGGAAGGAGAACCCTG
	Tas2r113	F:AGAATATGCAGCACACCGCC	R:CAATGATGGTTTGCAGGGCTC
	Tas2r114	F:ACACATCTTGGCAGATCCACA	R:TTTGATTCCATCTGCCTGCGA
	Tas2r115	F:CCTTTGGTGTATCCTTGATAGCTT	R:CTGCATCTTCCTTACATGTTTCA
	Tas2r116	F:AAGGTTTGGAGTGCTCTGCT	R: AGCTGTTCTTGCAACCTGTGT
	Tas2r117	F:CCCTGTGGACACATCACAAG	R:TCACAGTTTGTAGGGCTTTGAA
	Tas2r118	F:CACTGGGTGCAGATGAAACA	R: CTTCAGAACAGTGAACTGAGCTTT
	Tas2r119	F:TGCACAGCTGGGTCTATCCT	R:CACCAAGCCATGTGGCAAAC
	Tas2r120	F:TTGGTTTGTTGTGGGCAATGT	R:TCAGTATGGTCCCCAGCCAA
	Tas2r121	F:CTGGTCTTATTGGAGATGATTGTG	R:GGAGAAGATTAACAGGATGAAGGA
	Tas2r122	F:GCTTATTGTGGCAAGCTCCA	R:AACCTCCACAATGACACACCA
	Tas2r123	F:TTCATGCTGTGCCCACATTT	R:AAGACACCGAGGCATGTAGT
	Tas2r124	F:CTACGGCCCACAGAAATGCC	R:AGCTGCCTCATTACCCAAAGA
	Tas2r125	F:CTAAAGGCTCCGAAGACACCA	R:AACAGGAGAAAGGCCACTACC
	Tas2r126	F:GTGTGTGGGATTGGTCAACA	R:GCTCCCGGAGTACTCAACC
	Tas2r129	F:TTTAGCATGTGGCTTGCTGC	R:AGAGGCCCAAAGACATGAGC
	Tas2r130	F:TGCATTCATTGCACTGGTAAA	R:GATTAAATCAATAGAGGCAATCTTCC
	Tas2r131	F:TAGCCCACATTTCCCATCC	R:CAAGCACACCTCTCAATCTCC
	Tas2r134	F:GCCTGGGAAGTGGTAACCTA	R:GTTGCTTAGTATCAGAATGGTGGA
	Tas2r135	F:CCATCATGTCCACAGGAGAA	R:TCAGTAGTCTGACATCCAAGAACTGT
	Tas2r136	F: GGACAATGAGGCTTTATGGAA	R:CCTTAATGTGGGTTGAAGCAC
	Tas2r137	F:CTGGCTCAAATGGAGAGCTT	R:GGTACTGACACAGGATAAGAGCAG
	Tas2r138	F:CAAACCAAGTGAGCCTCTGG	R:GAGAAGCGGACAATCTTGGA
	Tas2r139	F:ATGGCTCAACCCAGCAACTAC	R:ACAGCCATGACAATCCCACT
	Tas2r140	F:GAAGAACATGCAACACAATGC	R:AGGGCCTTAATATGGGCTGT
	Tas2r143	F:CATTGGCCTCTATGTTGCAG	R:TGTCCGGTTCCTCATCCA
	Tas2r144	F:AAGCAGAAAATCATAGGGCTGA	R:TGAAGGAAACCAACACTGACA
	Gsdma	F:CTAGTCTGATCCTTCCCATGTGT	R:CAGTGTGGGCAGTAACGTGT
	Gsdma2	F:CCCTTCCCTGGAAAATCTGGA	R:CCGGGTGACATCCTCAAACA
	Gsdma3	F:ACTGAAATGCCTGCTCATCTT	R:CATCAGGAGATGGGCTTAGTGG
	Gsdmc	F:TCTTCCCGGTTGGCTTTGAAA	R:AGGACTTAACAAACCCTGCTTC
	Gsdmc2	F:CTGTGGAATGCTTGTCCGATG	R:CCTCCAGGTCCGTTGATTGG
	Gsdmc3	F:AGCCCGCCCATCTAGATTTC	R:TGCCCCAACTGACTCAACTC
	Gsdmc4	F:TGAGGAGCCTGCCAATCTAAA	R:ATGTGGGGTGCTAGAATCCTT
	Gsdmd	F:GATCAAGGAGGTAAGCGGCA	R:CACTCCGGTTCTGGTTCTGG
	Gsdme	F:GTCAGCAGAGGCAAACAATCG	R:TTTCTTCGCTGTGCTGCTTG
	Tlr4	F:GTTCTCTCATGGCCTCCACT	R:AGGGACTTTGCTGAGTTTCTGAT

Continued on next page

Continued

Species	Gene name	Sequences(5’-3’)	Sequences(5’-3’)
Mouse	Nlrp3	F:CCCCTTTATTTGTACCCAAGGCT	R:GCAACGGACACTCGTCATCT
	Asc	F:GACAGTACCAGGCAGTTCGT	R:AGTCCTTGCAGGTCAGGTTC
	Casp1	F:CCGCGGTTGAATCCTTTTCAG	R:TGTGCGCATGTTTCTTTCCC
	Il-1b	F:TGCCACCTTTTGACAGTGATG	R:AAGGTCCACGGGAAAGACAC
	Col1a1	F:AGAGCGGAGAGTACTGGATCG	R:TCGAACGGGAATCCATCGGT
	Fn1	F:AACAGAAATTGACAAGCCGTC	R:TCTGTTTGATCTGGACTGGCA
	Timp1	F:GCAAAGAGCTTTCTCAAAGACC	R:AGGGATAGATAAACAGGGAAACACT

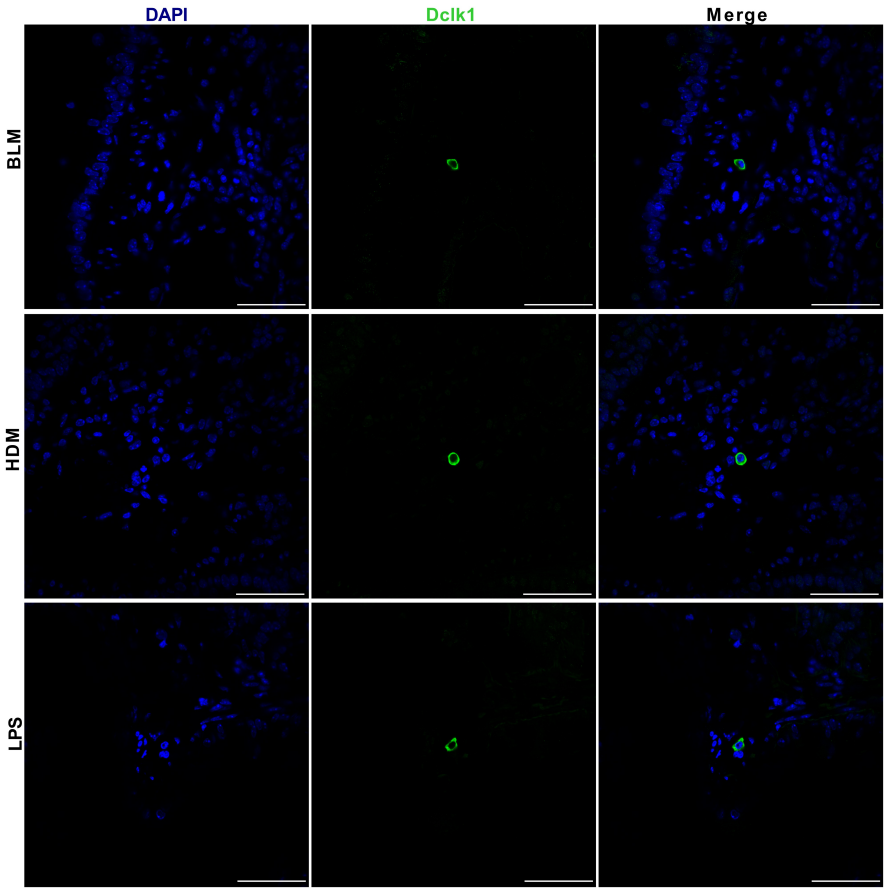

Figure 1—figure supplement 1. Chemically induced severe injury also engenders ectopic formation of lung tuft cells.

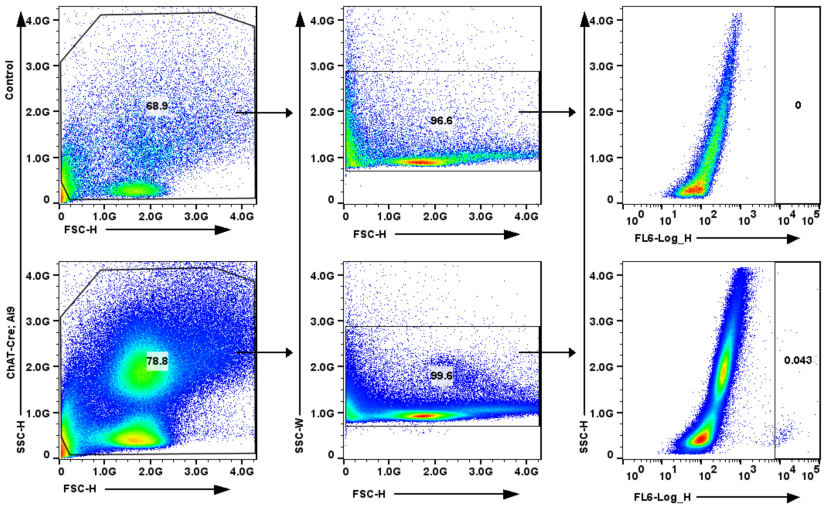

Figure 2—figure supplement 1. FACs sorting of ectopic tuft cells.

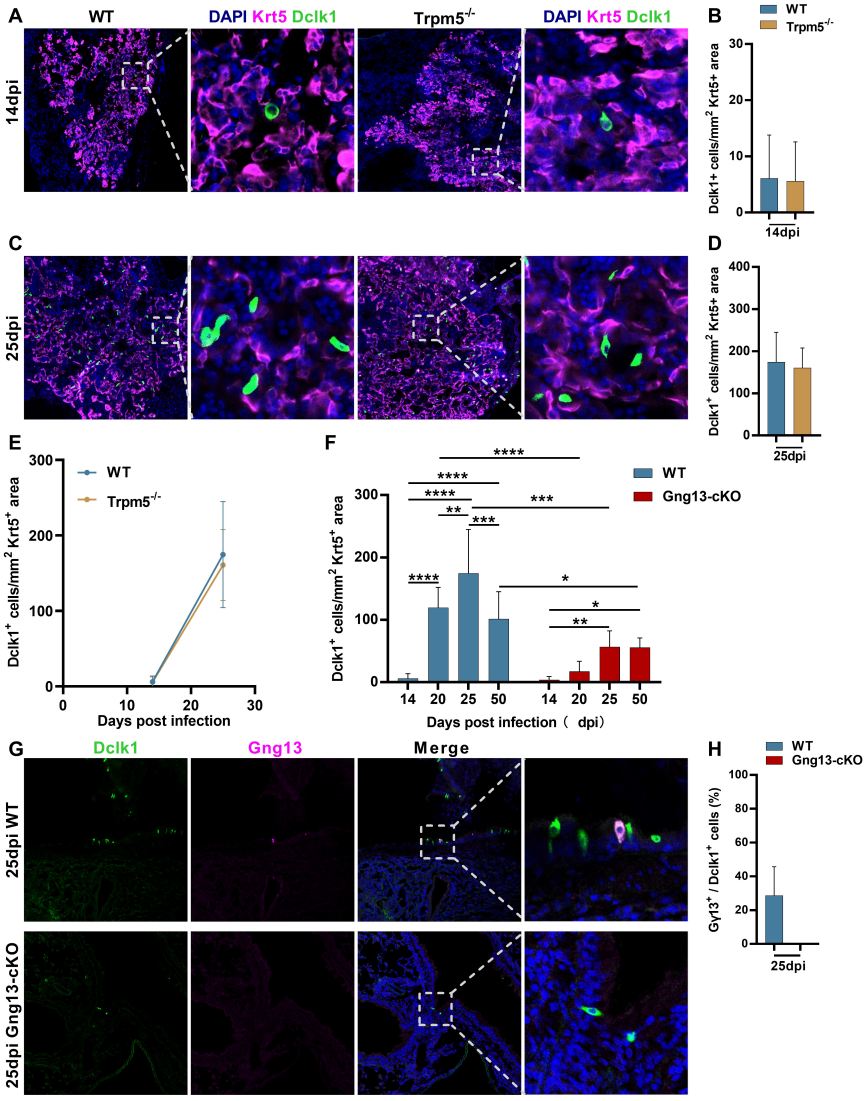

Figure 3—figure supplement 1. Ectopic generation of tuft cells in WT, *Trpm5*$^{-/-}$ and *Gng13*-cKO mice over days post infection.

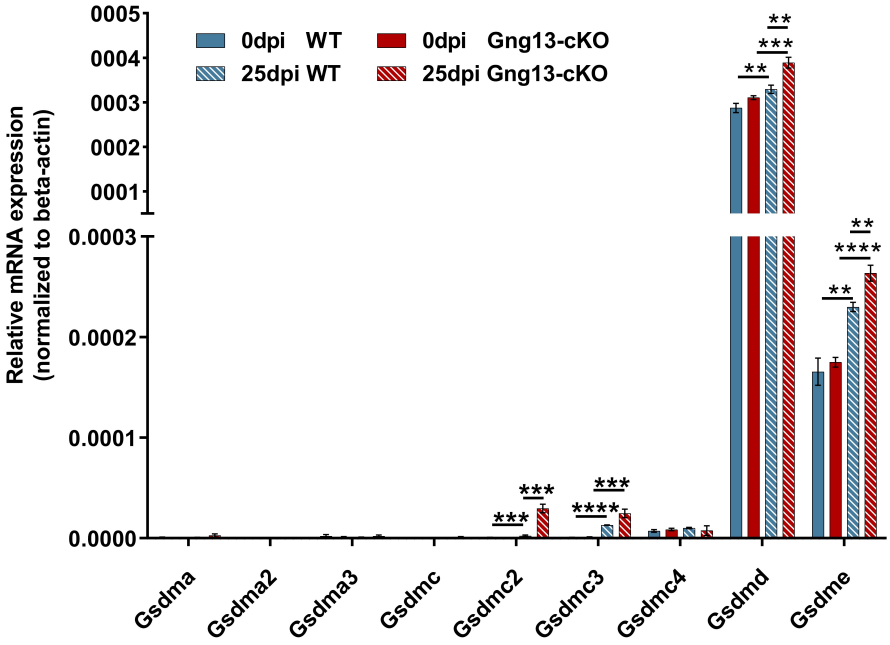

Figure 4—figure supplement 1. qRT-PCR analysis of gasdermin gene expression in WT and *Gng13*-cKO lungs.

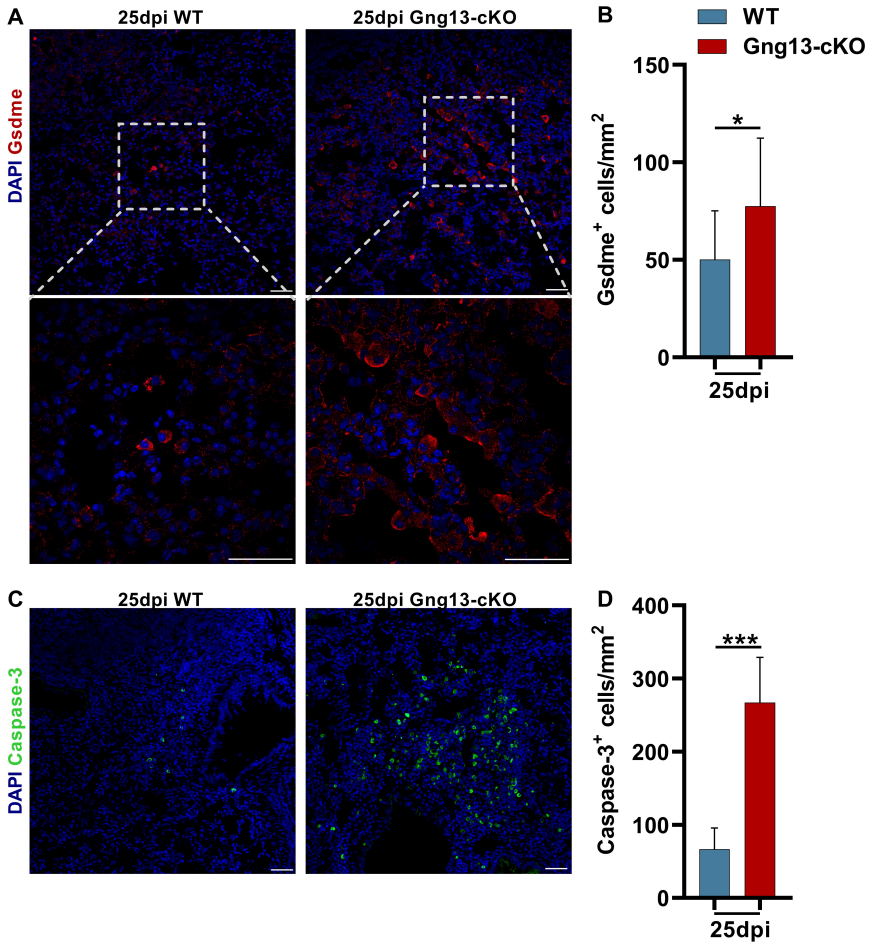

Figure 5—figure supplement 1. Expression of gasdermin E and caspase 3 in the H1N1-injured lungs.

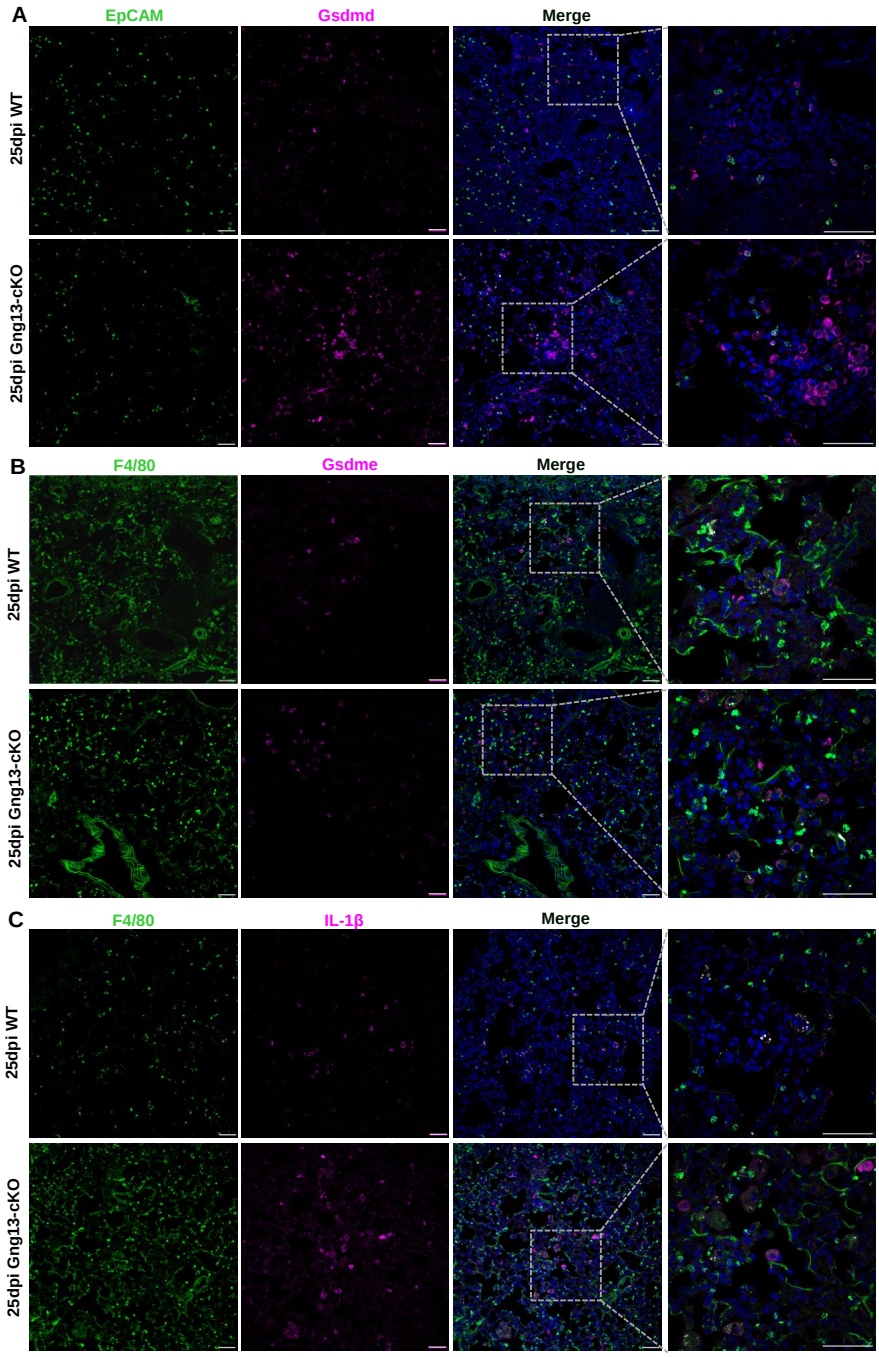

Figure 5—figure supplement 2. Partial colocalization of gasdermin D, E and *IL-1β* to epithelial cells and macrophages.